PHYSICAL REVIEW D **71,** 092003 (2005)

Dalitz analysis of the three-body charmless decays $B^+ \to K^+\pi^+\pi^-$ and $B^+ \to K^+K^+K^-$

A. Garmash,[32] K. Abe,[7] K. Abe,[40] H. Aihara,[42] M. Akatsu,[20] Y. Asano,[46] V. Aulchenko,[1] T. Aushev,[11] T. Aziz,[38] S. Bahinipati,[4] A. M. Bakich,[37] Y. Ban,[31] I. Bedny,[1] U. Bitenc,[12] I. Bizjak,[12] S. Blyth,[24] A. Bondar,[1] A. Bozek,[25] M. Bračko,[7,18,12] J. Brodzicka,[25] P. Chang,[24] Y. Chao,[24] A. Chen,[22] K.-F. Chen,[24] B. G. Cheon,[3] R. Chistov,[11] S.-K. Choi,[5] Y. Choi,[36] Y. K. Choi,[36] A. Chuvikov,[32] J. Dalseno,[19] M. Danilov,[11] M. Dash,[47] L. Y. Dong,[9] J. Dragic,[19] A. Drutskoy,[4] S. Eidelman,[1] V. Eiges,[11] Y. Enari,[20] S. Fratina,[12] N. Gabyshev,[1] T. Gershon,[7] G. Gokhroo,[38] J. Haba,[7] T. Hara,[29] N. C. Hastings,[7] K. Hayasaka,[20] H. Hayashii,[21] M. Hazumi,[7] T. Higuchi,[7] L. Hinz,[16] T. Hokuue,[20] Y. Hoshi,[40] S. Hou,[22] W.-S. Hou,[24] T. Iijima,[20] A. Imoto,[21] K. Inami,[20] A. Ishikawa,[7] R. Itoh,[7] M. Iwasaki,[42] Y. Iwasaki,[7] J. H. Kang,[48] J. S. Kang,[14] S. U. Kataoka,[21] N. Katayama,[7] H. Kawai,[2] T. Kawasaki,[27] H. R. Khan,[43] H. Kichimi,[7] H. J. Kim,[15] J. H. Kim,[36] S. K. Kim,[35] S. M. Kim,[36] K. Kinoshita,[4] P. Koppenburg,[7] S. Korpar,[18,12] P. Križan,[17,12] P. Krokovny,[1] R. Kulasiri,[4] C. C. Kuo,[22] A. Kuzmin,[1] Y.-J. Kwon,[48] T. Lesiak,[25] J. Li,[34] S.-W. Lin,[24] D. Liventsev,[11] G. Majumder,[38] F. Mandl,[10] D. Marlow,[32] T. Matsumoto,[44] A. Matyja,[25] W. Mitaroff,[10] H. Miyake,[29] H. Miyata,[27] R. Mizuk,[11] D. Mohapatra,[47] T. Mori,[43] T. Nagamine,[41] Y. Nagasaka,[8] E. Nakano,[28] M. Nakao,[7] H. Nakazawa,[7] Z. Natkaniec,[25] S. Nishida,[7] O. Nitoh,[45] S. Ogawa,[39] T. Ohshima,[20] T. Okabe,[20] S. Okuno,[13] S. L. Olsen,[6] W. Ostrowicz,[25] H. Ozaki,[7] P. Pakhlov,[11] H. Palka,[25] H. Park,[15] N. Parslow,[37] L. S. Peak,[37] R. Pestotnik,[12] L. E. Piilonen,[47] A. Poluektov,[1] M. Rozanska,[25] H. Sagawa,[7] Y. Sakai,[7] N. Sato,[20] T. Schietinger,[16] O. Schneider,[16] P. Schönmeier,[41] J. Schümann,[24] C. Schwanda,[10] A. J. Schwartz,[4] S. Semenov,[11] K. Senyo,[20] H. Shibuya,[39] B. Shwartz,[1] J. B. Singh,[30] A. Somov,[4] N. Soni,[30] R. Stamen,[7] S. Stanič,[46] M. Starič,[12] T. Sumiyoshi,[44] S. Suzuki,[33] S. Y. Suzuki,[7] O. Tajima,[7] F. Takasaki,[7] K. Tamai,[7] N. Tamura,[27] M. Tanaka,[7] Y. Teramoto,[28] X. C. Tian,[31] K. Trabelsi,[6] T. Tsukamoto,[7] S. Uehara,[7] T. Uglov,[11] K. Ueno,[24] S. Uno,[7] Y. Ushiroda,[7] G. Varner,[6] K. E. Varvell,[37] S. Villa,[16] C. C. Wang,[24] C. H. Wang,[23] M.-Z. Wang,[24] M. Watanabe,[27] Y. Watanabe,[43] A. Yamaguchi,[41] H. Yamamoto,[41] Y. Yamashita,[26] J. Ying,[31] Y. Yusa,[41] C. C. Zhang,[9] L. M. Zhang,[34] Z. P. Zhang,[34] V. Zhilich,[1] and D. Žontar[17,12]

(Belle Collaboration)

[1]*Budker Institute of Nuclear Physics, Novosibirsk*
[2]*Chiba University, Chiba*
[3]*Chonnam National University, Kwangju*
[4]*University of Cincinnati, Cincinnati, Ohio 45221, USA*
[5]*Gyeongsang National University, Chinju*
[6]*University of Hawaii, Honolulu, Hawaii 96822, USA*
[7]*High Energy Accelerator Research Organization (KEK), Tsukuba*
[8]*Hiroshima Institute of Technology, Hiroshima*
[9]*Institute of High Energy Physics, Chinese Academy of Sciences, Beijing*
[10]*Institute of High Energy Physics, Vienna*
[11]*Institute for Theoretical and Experimental Physics, Moscow*
[12]*J. Stefan Institute, Ljubljana*
[13]*Kanagawa University, Yokohama*
[14]*Korea University, Seoul*
[15]*Kyungpook National University, Taegu*
[16]*Swiss Federal Institute of Technology of Lausanne, EPFL, Lausanne*
[17]*University of Ljubljana, Ljubljana*
[18]*University of Maribor, Maribor*
[19]*University of Melbourne, Victoria*
[20]*Nagoya University, Nagoya*
[21]*Nara Women's University, Nara*
[22]*National Central University, Chung-li*
[23]*National United University, Miao Li*
[24]*Department of Physics, National Taiwan University, Taipei*
[25]*H. Niewodniczanski Institute of Nuclear Physics, Krakow*
[26]*Nihon Dental College, Niigata*
[27]*Niigata University, Niigata*
[28]*Osaka City University, Osaka*
[29]*Osaka University, Osaka*
[30]*Panjab University, Chandigarh*

1550-7998/2005/71(9)/092003(24)$23.00

[31]*Peking University, Beijing*
[32]*Princeton University, Princeton, New Jersey 08544, USA*
[33]*Saga University, Saga*
[34]*University of Science and Technology of China, Hefei*
[35]*Seoul National University, Seoul*
[36]*Sungkyunkwan University, Suwon*
[37]*University of Sydney, Sydney NSW*
[38]*Tata Institute of Fundamental Research, Bombay*
[39]*Toho University, Funabashi*
[40]*Tohoku Gakuin University, Tagajo*
[41]*Tohoku University, Sendai*
[42]*Department of Physics, University of Tokyo, Tokyo*
[43]*Tokyo Institute of Technology, Tokyo*
[44]*Tokyo Metropolitan University, Tokyo*
[45]*Tokyo University of Agriculture and Technology, Tokyo*
[46]*University of Tsukuba, Tsukuba*
[47]*Virginia Polytechnic Institute and State University, Blacksburg, Virginia 24061, USA*
[48]*Yonsei University, Seoul*

(Received 23 December 2004; published 20 May 2005)

We report results on the Dalitz analysis of three-body charmless $B^+ \to K^+\pi^+\pi^-$ and $B^+ \to K^+K^+K^-$ decays based on a 140 fb^{-1} data sample collected with the Belle detector. Measurements of branching fractions for quasi-two-body decays to scalar-pseudoscalar states: $B^+ \to f_0(980)K^+$, $B^+ \to K_0^*(1430)^0\pi^+$, and to vector-pseudoscalar states: $B^+ \to K^*(892)^0\pi^+$, $B^+ \to \rho^0K^+$, $B^+ \to \phi K^+$ are presented. Upper limits on decays to some pseudoscalar-tensor final states are reported. We also report the measurement of the $B^+ \to \chi_{c0}K^+$ branching fraction in two χ_{c0} decays channels: $\chi_{c0} \to \pi^+\pi^-$ and $\chi_{c0} \to K^+K^-$.

DOI: 10.1103/PhysRevD.71.092003 PACS numbers: 13.20.He, 13.25.Hw, 13.30.Eg, 14.40.Nd

I. INTRODUCTION

Studies of B meson decays to three-body charmless hadronic final states are a natural extension of studies of decays to two-body charmless final states. Some of the final states considered so far as two-body (for example $\rho\pi$, $K^*\pi$, etc.) proceed via quasi-two-body processes involving a wide resonance state that immediately decays in the simplest case to two particles, thereby producing a three-body final state. Multiple resonances occurring nearby in phase space will interfere and a full amplitude analysis is required to extract correct branching fractions for the intermediate quasi-two-body states. B meson decays to three-body charmless hadronic final states may provide new possibilities for CP violation searches [1–4].

Observations of B meson decays to various three-body charmless hadronic final states have already been reported by the Belle [3,5,6], CLEO [7], and BaBar [8] Collaborations. First results on the distribution of signal events over the Dalitz plot in the three-body $B^+ \to K^+\pi^+\pi^-$ and $B^+ \to K^+K^+K^-$ decays are described in Ref. [6]. With a data sample of 29.1 fb^{-1} a simplified analysis technique was used due to lack of statistics. Using a similar technique, the BaBar Collaboration has reported results of their analysis of the Dalitz plot for the decay $B^+ \to K^+\pi^+\pi^-$ with a 56.4 fb^{-1} data sample [9]. With the large data sample that is now available, we can perform a full amplitude analysis. The analysis described in this paper is based on a 140 fb^{-1} data sample containing 152×10^6 $B\bar{B}$ pairs, collected with the Belle detector operating at the KEKB asymmetric-energy e^+e^- collider [10] with a center-of-mass (c.m.) energy at the $\Upsilon(4S)$ resonance (on-resonance data). The beam energies are 3.5 GeV for positrons and 8.0 GeV for electrons. For the study of the $e^+e^- \to q\bar{q}$ continuum background, we use 8.3 fb^{-1} of data taken 60 MeV below the $\Upsilon(4S)$ resonance (off-resonance data).

The paper is organized as follows: Section II gives a brief description of the Belle detector; the event reconstruction procedure and background suppression techniques are described in Secs. III and IV, respectively; Section V describes results on the three-body signal yields measurement and qualitative analysis of the two-particle mass spectra, while Sec. VI is devoted to the amplitude analysis of the observed three-body signals; final results of the analysis are given in Sec. VII and discussed in Sec. VIII.

II. THE BELLE DETECTOR

The Belle detector [11] is a large-solid-angle magnetic spectrometer based on a 1.5 T superconducting solenoid magnet. Charged particle tracking is provided by a three-layer silicon vertex detector and a 50-layer central drift chamber (CDC) that surround the interaction point. The charged particle acceptance covers laboratory polar angles

---

[*] On leave from Nova Gorica Polytechnic, Nova Gorica.

between $\theta = 17°$ and $150°$, corresponding to about 92% of the total solid angle in the c.m. frame. The momentum resolution is determined from cosmic rays and $e^+e^- \to \mu^+\mu^-$ events to be $\sigma_{p_t}/p_t = (0.30 \oplus 0.19 p_t)\%$, where p_t is the transverse momentum in GeV/c.

Charged hadron identification is provided by dE/dx measurements in the CDC, an array of 1188 aerogel Čerenkov counters (ACC), and a barrel-like array of 128 time-of-flight scintillation counters (TOF); information from the three subdetectors is combined to form a single likelihood ratio, which is then used for pion, kaon and proton discrimination. At large momenta (> 2.5 GeV/c) only the ACC and CDC are used to separate charged pions and kaons since here the TOF provides no additional discrimination. Electromagnetic showering particles are detected in an array of 8736 CsI(Tl) crystals (ECL) that covers the same solid angle as the charged particle tracking system. The energy resolution for electromagnetic showers is $\sigma_E/E = (1.3 \oplus 0.07/E \oplus 0.8/E^{1/4})\%$, where E is in GeV. Electron identification in Belle is based on a combination of dE/dx measurements in the CDC, the response of the ACC, and the position, shape and total energy deposition (i.e., E/p) of the shower detected in the ECL. The electron identification efficiency is greater than 92% for tracks with $p_{\mathrm{lab}} > 1.0$ GeV/c and the hadron misidentification probability is below 0.3%. The magnetic field is returned via an iron yoke that is instrumented to detect muons and K_L^0 mesons. We use a GEANT-based Monte Carlo (MC) simulation to model the response of the detector and determine its acceptance [12].

III. EVENT RECONSTRUCTION

Charged tracks are selected with a set of track quality requirements based on the number of CDC hits and on the distances of closest approach to the interaction point (IP). We also require that the track momenta transverse to the beam be greater than 0.1 GeV/c to reduce the low momentum combinatorial background. For charged kaon identification, we impose a requirement on the particle identification variable that has 86% efficiency and a 7% fake rate from misidentified pions. Charged tracks that are positively identified as electrons or protons are excluded. Since the muon identification efficiency and fake rate vary significantly with the track momentum, we do not veto muons to avoid additional systematic errors.

We identify B candidates using two variables: the energy difference ΔE and the beam-energy constrained mass M_{bc}. ΔE is calculated as $\Delta E = E_B - E^*_{\mathrm{beam}} = (\sum_i \sqrt{c^2\mathbf{p}_i^2 + c^4 m_i^2}) - E^*_{\mathrm{beam}}$, where the summation is over all particles from a B candidate; and $\mathbf{p}_i$ and m_i are their c.m. three-momenta and masses, respectively. Since the $\Upsilon(4S)$ decays to a pair of B mesons with no additional particles, each B meson carries half of the c.m. energy $\sqrt{s}/2 = E^*_{\mathrm{beam}} = 5.29$ GeV, where E^*_{beam} is the beam energy in the c.m. frame. The ΔE distribution for the $B^+ \to K^+\pi^+\pi^-$ signal MC events is shown in Fig. 1(a). Since there are only charged particles in final states considered in this analysis, the ΔE width is governed by the track momentum resolution. A typical value of the ΔE resolution is 15 MeV. The beam-energy spread is about 3 MeV and gives a negligible contribution to the total ΔE width. The signal ΔE shape is fitted by a sum of two Gaussian functions with a common mean. In fits to the experimental data, we fix the width and fraction of the second Gaussian function from MC simulation. The width of the main Gaussian is floated. For comparison, the ΔE distribution for the off-resonance data is also shown in Fig. 1(a), where the background is parametrized by a linear function.

The beam-energy constrained mass variable M_{bc} is equivalent to the B invariant mass with the measured B candidate energy E_B replaced by the beam energy E^*_{beam}: $M_{\mathrm{bc}} = \frac{1}{c^2}\sqrt{E^{*2}_{\mathrm{beam}} - c^2\mathbf{P}_B^2} = \frac{1}{c^2}\sqrt{E^{*2}_{\mathrm{beam}} - c^2(\sum_i \mathbf{p}_i)^2}$, where $\mathbf{P}_B$ is the B candidate momentum in the c.m. frame. The average B meson momentum in the c.m. frame is about 0.34 GeV/c which is much smaller than its total energy.

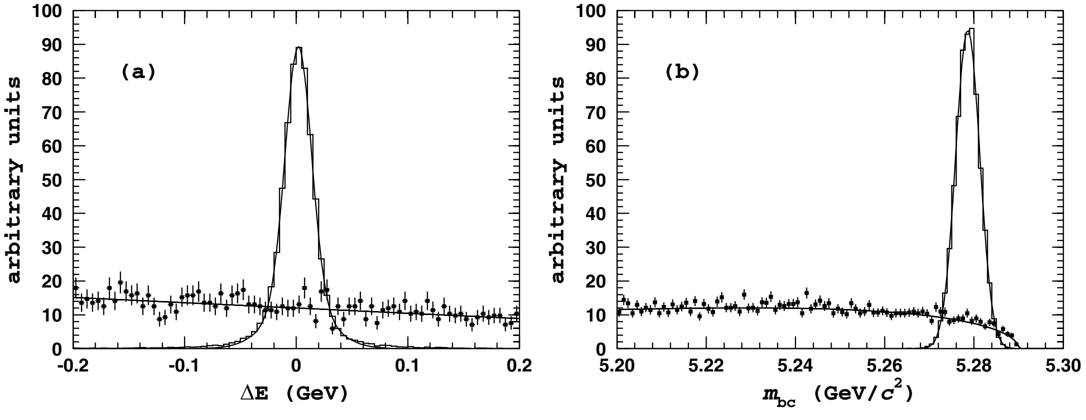

FIG. 1. (a) Energy difference ΔE and (b) beam constrained mass M_{bc} distributions for $B^+ \to K^+\pi^+\pi^-$ signal MC events (histograms) and $q\bar{q}$ background in off-resonance data (points). Curves represent the results of the fits.

Thus, the uncertainty in the measured $\mathbf{P}_B$ gives a small contribution to the $M_{\rm bc}$ width, which is dominated by the beam-energy spread. The $M_{\rm bc}$ width is about 3 MeV$/c^2$ and is nearly independent of the final state unless photons are included. The $M_{\rm bc}$ distribution for the signal $B^+ \to K^+\pi^+\pi^-$ MC events and for the off-resonance data are shown in Fig. 1(b). The signal $M_{\rm bc}$ shape is well described by a Gaussian function. The background shape is parametrized with an empirical function $f(M_{\rm bc}) \propto x\sqrt{1-x^2}\exp[-\lambda(1-x^2)]$, where $x = M_{\rm bc}/E^*_{\rm beam}$ and λ is a parameter [13].

IV. BACKGROUND SUPPRESSION

There are two sources of the background: the dominant one is due to $e^+e^- \to q\bar{q}$ ($q = u, d, s$ and c quarks) continuum events that have a cross-section about 3 times larger than that for the $e^+e^- \to \Upsilon(4S) \to B\bar{B}$; the other one originates from other B meson decays. The background from continuum events is suppressed using variables that characterize the event topology. Since the two B mesons produced from an $\Upsilon(4S)$ decay are nearly at rest in the c.m. frame, their decay products are uncorrelated and the event tends to be spherical. In contrast, hadrons from continuum $q\bar{q}$ events tend to exhibit a two-jet structure. We use $\theta_{\rm thr}$, which is the angle between the thrust axis of the B candidate and that of the rest of the event, to discriminate between the two cases. The distribution of $|\cos\theta_{\rm thr}|$ is strongly peaked near $|\cos\theta_{\rm thr}| = 1.0$ for $q\bar{q}$ events and is nearly flat for $B\bar{B}$ events. A Fisher discriminant is utilized for the further suppression of the continuum background. When combined, these two variables reject about 98% (92%) of the continuum background in the $B^+ \to K^+\pi^+\pi^-$ ($B^+ \to K^+K^+K^-$) decay while retaining 36% (70%) of the signal. (As the continuum background in the three-kaon final state is much smaller a looser requirement on the Fisher discriminant is imposed to retain the efficiency.) A detailed description of the continuum suppression technique can be found in Ref. [3] and references therein.

The understanding of the background that originates from other B meson decays is of great importance in the study of charmless B decays. We study the $B\bar{B}$ related background using a large sample (about 2.5 times the experimental dataset) of MC generated $B\bar{B}$ generic events. We use the CLEO generator [14] to simulate B decays governed by the dominant $b \to c$ tree transition. Note that charmless hadronic B decays that proceed via $b \to s(d)$ penguin and $b \to u$ tree transitions are not included in the generator and are generated separately. We find that the dominant $B\bar{B}$ background in the $K^+\pi^+\pi^-$ final state that peaks in the signal region is due to $B^+ \to \bar{D}^0\pi^+$, $\bar{D}^0 \to K^+\pi^-$ and also $B^+ \to J/\psi(\psi(2S))K^+$, $J/\psi(\psi(2S)) \to \mu^+\mu^-$ decays. We veto $B^+ \to \bar{D}^0\pi^+$ events by requiring $|M(K\pi) - M_D| > 0.10$ GeV$/c^2$. The $B^+ \to \bar{D}^0K^+$, $\bar{D}^0 \to \pi^+\pi^-$ signal is removed by requiring $|M(\pi^+\pi^-) - M_D| > 15$ MeV$/c^2$ ($\sim 2.5\sigma$). To suppress the background due to π/K misidentification, we also exclude candidates if the invariant mass of any pair of oppositely charged tracks from the B candidate is consistent with the $\bar{D}^0 \to K^+\pi^-$ hypothesis within 15 MeV$/c^2$, regardless of the particle identification information. Modes with $J/\psi(\psi(2S))$ in the final state contribute due to muon-pion misidentification; the contribution from the $J/\psi(\psi(2S)) \to e^+e^-$ submode is found to be negligible after the electron veto requirement. We exclude J/ψ and $\psi(2S)$ backgrounds by requiring $|M(\pi^+\pi^-)_{\mu^+\mu^-} - M_{J/\psi}| > 0.07$ GeV$/c^2$ and $|M(\pi^+\pi^-)_{\mu^+\mu^-} - M_{\psi(2S)}| > 0.05$ GeV$/c^2$, where subscript $\mu^+\mu^-$ indicates that the muon mass assignment was used for charged tracks to calculate the two-particle invariant mass. Yet another small but clearly visible background associated with $B^+ \to J/\psi K^+$, $J/\psi \to \mu^+\mu^-$ decays is due to a somewhat complicated particle misidentification pattern: the charged kaon is misidentified as a pion, the μ^+ is misidentified as a kaon and the μ^- as another pion. This background is excluded by applying a veto: $|M(K^+\pi^-)_{\mu^+\mu^-} - M_{J/\psi}| > 0.020$ GeV$/c^2$. The most significant background from charmless B decays is found to originate from $B^+ \to \eta' K^+$ followed by $\eta' \to \pi^+\pi^-\gamma$. Another contribution comes from $B^+ \to \rho^0\pi^+$ decay, where one of the final state pions is misidentified as a kaon. We take these contributions into account when determining the signal yield.

The dominant background to the $K^+K^+K^-$ final state from other B decays is found to come from the process $B \to Dh$, where h stands for a charged pion or kaon. To suppress this background, we reject events where any two-particle invariant mass is consistent with $\bar{D}^0 \to K^+K^-$ or $\bar{D}^0 \to K^+\pi^-$ within 15 MeV$/c^2$ regardless of the particle identification information. We find no charmless B decay modes that produce a significant background to the $K^+K^+K^-$ final state.

V. THREE-BODY SIGNAL YIELDS

The ΔE distributions for $B^+ \to K^+\pi^+\pi^-$ and $B^+ \to K^+K^+K^-$ candidates that pass all the selection requirements and with $|M_{\rm bc} - M_B| < 9$ MeV$/c^2$ are shown in Fig. 2, where clear peaks in the signal regions are observed. In the fit to the ΔE distribution for the $K^+\pi^+\pi^-$ final state, we fix the shape and normalization of the charmless $B\bar{B}$ background components from the measured branching fractions [15] and known number of produced $B\bar{B}$ events. For the $B\bar{B}$ generic component, we fix only the shape and let the normalization float. The slope and normalization of the $q\bar{q}$ background component are free parameters. Results of the fit are shown in Fig. 2, where different components of the background are shown separately for comparison. There is a large increase in the level of the $B\bar{B}$ related background in the $\Delta E < -0.15$ GeV region for the $K^+\pi^+\pi^-$ final state. This is mainly due to the decay $B \to D\pi$, $D \to K\pi\pi$. This decay mode produces the same final

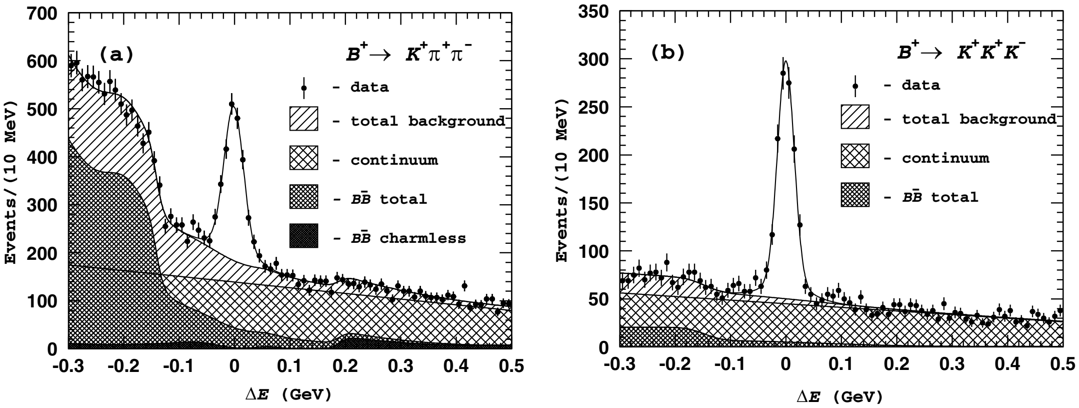

FIG. 2. ΔE distributions for (a) $B^+ \to K^+\pi^+\pi^-$ and (b) $B^+ \to K^+K^+K^-$ candidate events. Points with error bars are data; the curve is the fit result; the hatched area is the background.

TABLE I. Results of fits to the ΔE distributions with a double Gaussian for the signal (see Sec. III).

Final state	σ_1 MeV	σ_2 MeV	Fraction of the Main Gaussian	Signal yield (Events)
$K^+\pi^+\pi^-$	17.5 ± 0.9	35.0 (fixed)	0.84 (fixed)	1533 ± 69
$K^+K^+K^-$	14.0 ± 1.0	40.0 (fixed)	0.85 (fixed)	1089 ± 41

state as the studied process plus one extra pion that is not included in the energy difference calculation. The decay $B \to D\pi$, $D \to K\mu\nu_\mu$ also contributes due to muon-pion misidentification. The shape of this background is described well by the MC simulation. In the fit to the ΔE distribution for the $K^+K^+K^-$ final state, we fix not only the shape but also the normalization of the $B\bar{B}$ background. This is done because the $B\bar{B}$ background in this final state is found to be much smaller than the dominant $q\bar{q}$ background, thus the relative fraction of these two contributions is poorly determined from the fit. The signal yields obtained from fits are given in Table I.

To examine possible quasi-two-body intermediate states in the observed $B^+ \to K^+\pi^+\pi^-$ and $B^+ \to K^+K^+K^-$ signals, we analyze two-particle invariant mass spectra. To determine the distribution of the background we use events in the $M_{\rm bc}$ and ΔE sidebands. The definition of the signal and sideband regions is illustrated in Fig. 3. Defined in this way, the $M_{\rm bc} - \Delta E$ sidebands are equivalent to the following sidebands in terms of the three-particle invariant mass $M(Khh)$ and three-particle momentum $P(Khh)$ in the c.m. frame:

$$0.05\ {\rm GeV}/c^2 < |M(Khh) - M_B| < 0.10\ {\rm GeV}/c^2; \quad P(Khh) < 0.48\ {\rm GeV}/c$$

and

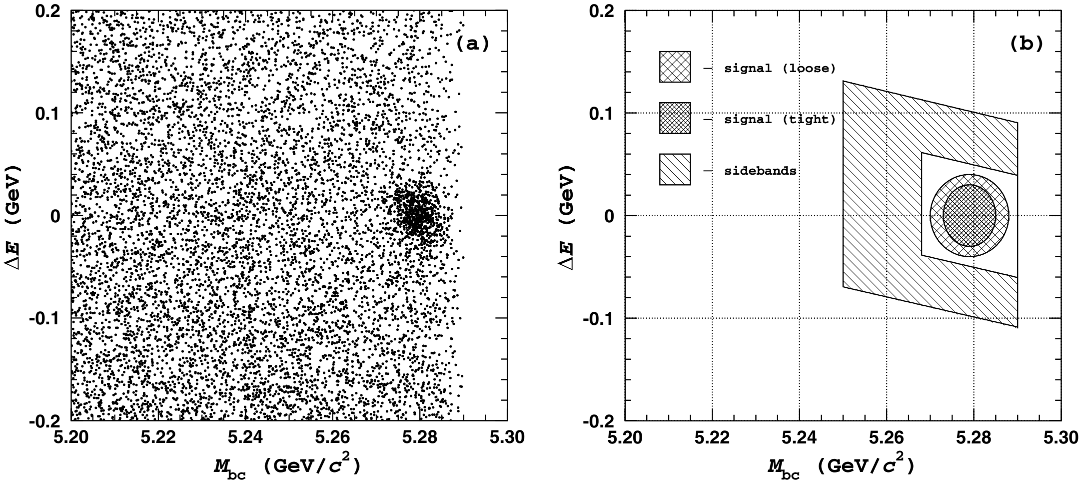

FIG. 3. (a) Distribution of ΔE versus $M_{\rm bc}$ for the $B^+ \to K^+K^+K^-$ candidates in data. (b) Definitions of the signal and sideband regions in the $M_{\rm bc} - \Delta E$ plane.

$$|M(Khh) - M_B| < 0.10\ \mathrm{GeV}/c^2;$$

$$0.48\mathrm{GeV}/c < P(Khh) < 0.65\ \mathrm{GeV}/c.$$

The signal region is defined as an ellipse around the $M_{\rm bc}$ and ΔE mean values:

$$\frac{(M_{\rm bc} - M_B)^2}{(n\sigma_{M_{\rm bc}})^2} + \frac{\Delta E^2}{(n\sigma_{\Delta E})^2} < 1,$$

where $\sigma_{M_{\rm bc}} = 3\ \mathrm{MeV}/c^2$ and $\sigma_{\Delta E}$ is equivalent to σ_1 in Table I. We define two signal regions: with loose ($n = 3$) and tight ($n = 2$) requirements. Tight requirements reduce (compared to the loose requirements) the background fraction in the data sample by about 65% while retaining about 85% of the signal. The efficiency of the loose (tight) requirements that define the signal region is 0.923 (0.767) for the $K^+\pi^+\pi^-$ final state and 0.948 (0.804) for the $K^+K^+K^-$ final state. The total number of events in the signal region is 2584 (1809) for the $K^+\pi^+\pi^-$ and 1400 (1078) for the $K^+K^+K^-$ final state. To determine the relative fraction of signal and background events in these samples, we use the results of the fits to the ΔE distributions (see Table I). We find 1533 ± 69 signal $B^+ \to K^+\pi^+\pi^-$ events and 1089 ± 41 signal $B^+ \to K^+K^+K^-$ events. The relative fraction of signal events in the signal region with loose (tight) requirements is then determined to be 0.548 ± 0.025 (0.650 ± 0.032) for the $K^+\pi^+\pi^-$ and 0.738 ± 0.028 (0.828 ± 0.033) for the $K^+K^+K^-$ final state. All final results are obtained from fits to events in the signal region with loose ΔE and $M_{\rm bc}$ requirements. The subsample with tight requirements is used for a cross-check only.

The $K^+\pi^-$ and $\pi^+\pi^-$ invariant mass spectra for $B^+ \to K^+\pi^+\pi^-$ candidate events in the $M_{\rm bc} - \Delta E$ loose signal region are shown as open histograms in Fig. 4. The hatched histograms show the corresponding spectra for background events in the $M_{\rm bc} - \Delta E$ sidebands, normalized to the estimated number of background events. To suppress the feed-across between the $\pi^+\pi^-$ and $K^+\pi^-$ resonance states, we require the $K^+\pi^-$ ($\pi^+\pi^-$) invariant mass to be larger than 2.0(1.5) GeV/c^2 when making the $\pi^+\pi^-$ ($K^+\pi^-$) projection. The $K^+\pi^-$ invariant mass spectrum is characterized by a narrow peak around 0.9 GeV/c^2, which is identified as the $K^*(892)^0$, and a broad enhancement around 1.4 GeV/c^2. Possible candidates for this enhancement are the scalar $K_0^*(1430)$ and tensor $K_2^*(1430)$ resonances. In the $\pi^+\pi^-$ invariant mass spectrum two distinct structures in the low mass region are observed. One is slightly below 1.0 GeV/c^2 and is consistent with the $f_0(980)$ and the other is between 1.0 GeV/c^2 and 1.5 GeV/c^2. We cannot identify unambiguously the resonant state that is responsible for such a structure. Possible candidates for a resonant state in this mass region might be $f_0(1370)$, $f_2(1270)$ and perhaps $\rho(1450)$ [15]. In what follows, we refer to this structure as $f_X(1300)$. There is also an indication for the $\rho(770)^0$. Finally, there is a clear signal for the decay $B^+ \to \chi_{c0}K^+$, $\chi_{c0} \to \pi^+\pi^-$. Figure 4(c) shows the $\pi^+\pi^-$ invariant mass distributions in the χ_{c0} mass region.

The K^+K^- invariant mass spectra for $B^+ \to K^+K^+K^-$ candidate events in the $M_{\rm bc} - \Delta E$ signal region with loose requirements are shown as open histograms in Fig. 5. Since there are two same-charge kaons in the $B^+ \to K^+K^+K^-$ decay, we distinguish the K^+K^- combinations with smaller, $M(K^+K^-)_{\rm min}$, and larger, $M(K^+K^-)_{\rm max}$, invariant masses. The $M(K^+K^-)_{\rm min}$ spectrum, shown in Fig. 5(a), is characterized by a narrow peak at 1.02 GeV/c^2 corresponding to the $\phi(1020)$ meson and a broad structure around 1.5 GeV/c^2, shown in Fig. 5(b). Possible candidates for a resonant state in this mass region are the $f_0(1370)$, $f_0(1500)$, or $f_2'(1525)$ [15]. In what follows, we refer to this structure as $f_X(1500)$. Figure 5(c) shows the $M(K^+K^-)_{\rm max}$ invariant mass distribution in the χ_{c0} mass region. A clear enhancement is observed at 3.4 GeV/c^2, where the χ_{c0} is expected. Some enhancement of signal events over the expected background level is also observed in the full mass range shown in Fig. 5(c). As the χ_{c0} meson has a significant natural width (about 15 MeV/c^2) [15], the amplitude that is responsible for the $B^+ \to \chi_{c0}K^+$ decay may interfere with a charmless amplitude. As a result of the interference between these two amplitudes, the lineshape of the χ_{c0} resonance can

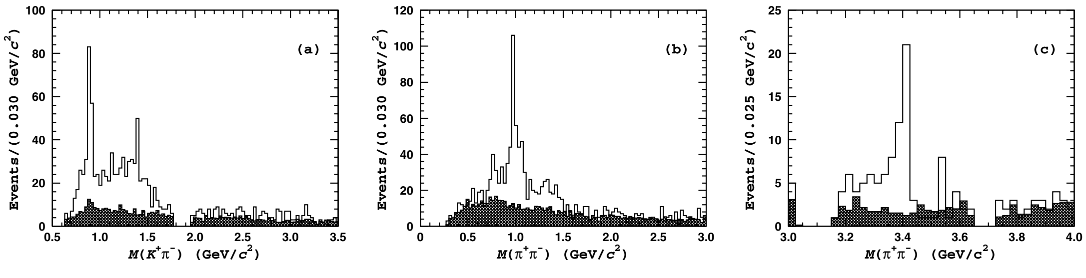

FIG. 4. Two-particle invariant mass spectra for $B^+ \to K^+\pi^+\pi^-$ candidates in the B signal region (open histograms) and for background events in the $\Delta E - M_{\rm bc}$ sidebands (hatched histograms). (a) $M(K^+\pi^-)$ spectrum with $M(\pi^+\pi^-) > 1.5\ \mathrm{GeV}/c^2$; (b) $M(\pi^+\pi^-)$ with $M(K^+\pi^-) > 2.0\ \mathrm{GeV}/c^2$ and (c) $M(\pi^+\pi^-)$ in the χ_{c0} mass region with $M(K^+\pi^-) > 2.0\ \mathrm{GeV}/c^2$.

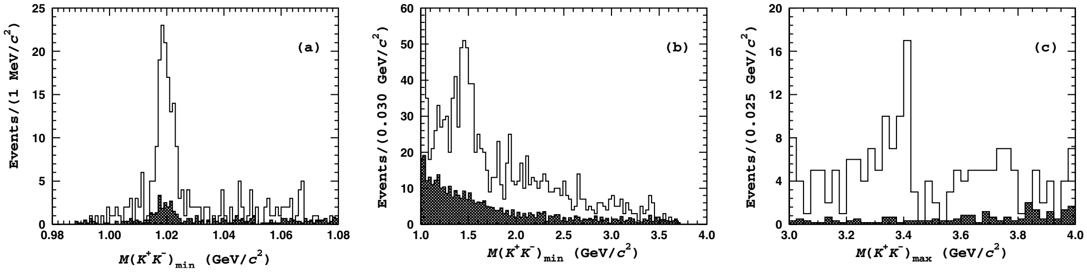

FIG. 5. Two-particle invariant mass spectra for $B^+ \to K^+K^+K^-$ candidates in the B signal region (open histograms) and for background events in the $\Delta E - M_{\rm bc}$ sidebands (hatched histograms). (a) $M(K^+K^-)_{\rm min}$ invariant mass spectrum near the $\phi(1020)$ mass region; (b) $M(K^+K^-)_{\rm min}$ spectrum in the full range; (c) $M(K^+K^-)_{\rm max}$ in the χ_{c0} mass region with 2.0 GeV/$c^2 < M(K^+K^-)_{\rm min} <$ 3.4 GeV/c^2.

be distorted. In our previous analysis of B meson decays to three-body charmless hadronic final states [3,6], we imposed a requirement on the invariant mass of the $\pi^+\pi^-$ and K^+K^- combination to veto the $B^+ \to \chi_{c0}K^+$ signal. In this analysis we do not apply such a requirement.

From these qualitative considerations it is apparent that an amplitude analysis is required for a more complete understanding of the individual quasi-two-body channels that contribute to the observed three-body $B^+ \to K^+\pi^+\pi^-$ and $B^+ \to K^+K^+K^-$ signals.

VI. AMPLITUDE ANALYSIS

In the preceding section we found that a significant fraction of the signals observed in $B^+ \to K^+\pi^+\pi^-$ and $B^+ \to K^+K^+K^-$ decays can be assigned to quasi-two-body intermediate states. These resonances will cause a nonuniform distribution of events in phase space that can be analyzed using the technique pioneered by Dalitz [16]. Multiple resonances that occur nearby in phase space will interfere and provide an opportunity to measure both the amplitudes and relative phases of the intermediate states. This in turn allows us to deduce their relative branching fractions. Amplitude analyses of various three-body D meson decays have been successfully performed by a number of groups [17]. From their results we can learn that this kind of analysis requires, in general, high statistics (of the order of a few thousand signal events, at least). In contrast to the analysis of D meson three-body decays, where the level of the combinatorial background is usually quite small, the signal and background levels in charmless three-body decays of B mesons are comparable. This complicates the analysis, requiring careful study of the distribution of background events over the phase space. Finally, independent of the statistics, the choice of the model (that is the set of quasi-two-body intermediate states) to fit the data is often not unique. This unavoidably introduces some model dependence into the determination of quasi-two-body branching fractions. This is especially true for three-body charmless decays of B mesons where experimental statistics is quite limited while the available phase space is large.

A. Formalism

Since we are studying the decay of a spin-zero particle to three spin-zero daughters $B \to h_1h_2h_3$, only 2 degrees of freedom are required to completely describe the kinematics. There are three invariant masses that can be formed by considering all possible pairs of final state particles: $s_{12} \equiv M^2(h_1h_2)$, $s_{13} \equiv M^2(h_1h_3)$ and $s_{23} \equiv M^2(h_2h_3)$. Only two of them are independent, however, since energy and momentum conservation results in the additional constraint

$$M^2 + m_1^2 + m_2^2 + m_3^2 = s_{12} + s_{13} + s_{23}, \qquad (1)$$

where M^2 is the mass of the initial particle, and m_i are masses of the daughter particles. In what follows we use s_{13} and s_{23} as the two independent variables.

The density of signal events on the Dalitz plot is described by the matrix element $\mathcal{M}$ as

$$d\Gamma = \frac{|\mathcal{M}|^2}{256\pi^3M^3}ds_{13}ds_{23}, \qquad (2)$$

which in turn depends on the decay dynamics.

The amplitude for B decay to a three-body final state via an intermediate resonance state R is given by

$$\mathcal{A}_J = F_BF_R^{(J)}BW_JT_J, \qquad (3)$$

where F_B and $F_R^{(J)}$ are form factors which, in general, are unknown functions. For $F_R^{(J)}$ we use the Blatt-Weisskopf penetration factors [18] given in Table II. These factors depend on a single parameter, R, which is the "radius" of the meson. For all intermediate resonances we set this parameter to $R = 1.5$ GeV^{-1}. Form factors are normalized to unity at the nominal meson mass. F_B is parametrized in a single pole approximation [19]

$$F_B = \frac{1}{1 - \frac{s}{M_{\rm pole}^2}}, \qquad (4)$$

where we use the mass of the B^* meson [15] as a pole mass $M_{\rm pole}$.

The Breit-Wigner function BW_J in Eq. (3) is given by the expression

TABLE II. Blatt-Weisskopf penetration form factors. p_r is the momentum of either daughter in the meson rest frame. p_s is the momentum of either daughter in the candidate rest frame (same as p_r except the parent mass used is the two-track invariant mass of the candidate rather than the mass of the meson). R is the meson radial parameter.

Spin J	Form factor $F_R^{(J)}$
0	1
1	$\frac{\sqrt{1+R^2p_r^2}}{\sqrt{1+R^2p_s^2}}$
2	$\frac{\sqrt{9+3R^2p_r^2+R^4p_r^4}}{\sqrt{9+3R^2p_s^2+R^4p_s^4}}$

$$BW_J(s) = \frac{1}{M_R^2 - s - iM_R\Gamma_R^{(J)}(s)}, \tag{5}$$

where M_R is the nominal mass of the resonance, and $\Gamma_R^{(J)}(s)$ is the "mass dependent width." In the general case, $\Gamma_R^{(J)}(s)$ is expressed as [20]

$$\Gamma_R^{(J)}(s) = \Gamma_R\left(\frac{p_s}{p_r}\right)^{2J+1}\left(\frac{M_R}{s^{1/2}}\right)F_R^2, \tag{6}$$

where p_r is the momentum of either daughter in the resonance rest frame, calculated with the resonance mass equal to the nominal M_R value, p_s is the momentum of either daughter in the resonance rest frame when the resonance mass is equal to $s^{1/2}$, J is the spin of the resonance, and Γ_R is the width of the resonance.

The function T_J in Eq. (3) describes the angular correlations between the B decay products. We distinguish the following three cases:

(1) *Scalar-pseudoscalar* ($J = 0$) *decay*—If R is a scalar state, the decay amplitude Eq. (3) takes the simplest form with $T_0 \equiv 1$. We treat the scalar $f_0(980)$ as a special case, for which we try two parametrizations for the s-dependent width $\Gamma_{f_0}(s)$: by Eq. (6), and following the parametrization by Flatté [21]

$$\Gamma_{f_0}(s) = \Gamma_\pi(s) + \Gamma_K(s), \tag{7}$$

where

$$\begin{aligned}\Gamma_\pi(s) &= g_\pi\sqrt{s/4 - m_\pi^2},\\ \Gamma_K(s) &= \frac{g_K}{2}\left(\sqrt{s/4 - m_{K^+}^2} + \sqrt{s/4 - m_{K^0}^2}\right),\end{aligned} \tag{8}$$

and g_π and g_K are coupling constants for $f_0(980) \to \pi\pi$ and $f_0(980) \to KK$, respectively.

(2) *Vector-pseudoscalar* ($J = 1$) *decay*—In the case of a pseudoscalar-vector decay of the B meson, the Lorentz-invariant expression for T_1 is given by

$$T_1(h_1h_2h_3|R_{23}) = s_{12} - s_{13} + \frac{(M^2 - m_1^2)(m_3^2 - m_2^2)}{s_{23}}, \tag{9}$$

where R_{23} is an intermediate resonance state decaying to h_2h_3 final state.

(3) *Tensor-pseudoscalar* ($J = 2$) *decay*—For a pseudoscalar-tensor decay, T_2 takes the form

$$\begin{aligned}T_2(h_1h_2h_3|R_{23}) = {}&\left(s_{13} - s_{12} + \frac{(M_B^2 - m_1^2)(m_2^2 - m_3^2)}{s_{23}}\right)^2\\ &- \frac{1}{3}\left(s_{23} - 2M_B^2 - 2m_1^2 + \frac{(M_B^2 - m_1^2)^2}{s_{23}}\right)\\ &\times\left(s_{23} - 2m_2^2 - 2m_3^2 + \frac{(m_2^2 - m_3^2)^2}{s_{23}}\right).\end{aligned} \tag{10}$$

We do not consider resonant states of higher spin in our analysis.

There is also the possibility of a so-called "nonresonant" amplitude. In the Dalitz analysis of D meson decays to three-body final states the nonresonant amplitude is often parametrized as a complex constant. In the case of B meson decays, where the available phase space is much larger, it is rather unlikely that the nonresonant amplitude will have a constant value over the entire phase space; some form factors should be introduced. Unfortunately, at the moment there is no theoretical consensus on the properties of nonresonant B meson decays. In our analysis we use an empirical parametrization that in the case of the $K^+\pi^+\pi^-$ final state is

$$\mathcal{A}_{\rm nr}(K^+\pi^+\pi^-) = a_1^{\rm nr}e^{-\alpha s_{13}}e^{i\delta_1^{\rm nr}} + a_2^{\rm nr}e^{-\alpha s_{23}}e^{i\delta_2^{\rm nr}}, \tag{11}$$

where $s_{13} \equiv M^2(K^+\pi^-)$, $s_{23} \equiv M^2(\pi^+\pi^-)$, and $a_{1,2}^{\rm nr}$, and $\delta_{1,2}^{\rm nr}$ and α are fit parameters. In a certain limit this parametrization is equivalent to a constant. Several alternative parametrizations (mentioned below) are also considered to estimate the model dependence.

An important feature that should be taken into account in the construction of the matrix element for the decay $B^+ \to K^+K^+K^-$ is the presence of the two identical kaons in the final state. This is achieved by symmetrizing the matrix element with respect to the interchange of the two kaons of the same charge, that is $s_{13} \leftrightarrow s_{23}$. Because of symmetrization the nonresonant amplitude for the $K^+K^+K^-$ final state becomes

$$\mathcal{A}_{\rm nr}(K^+K^+K^-) = a^{\rm nr}(e^{-\alpha s_{13}} + e^{-\alpha s_{23}})e^{i\delta^{\rm nr}}, \tag{12}$$

where $s_{13} \equiv M^2(K_1^+K^-)$, $s_{23} \equiv M^2(K_2^+K^-)$.

Given the amplitude for each decay type, the overall matrix elements can be written as a coherent sum

$$\mathcal{M} = \sum_j a_j e^{i\delta_j}\mathcal{A}^j + \mathcal{A}_{\rm nr}, \tag{13}$$

where the index j denotes the quasi-two-body intermediate state, a_j and δ_j are the amplitude and relative phase of the j-th component. Since we are sensitive only to the relative phases and amplitudes, we are free to fix one phase and one amplitude in Eq. (13). The fraction f_l of the total three-body signal attributed to a particular quasi-two-body intermediate state can be calculated as

$$f_l = \frac{\int |a_l \mathcal{A}^l|^2 ds_{13} ds_{23}}{\int |\mathcal{M}|^2 ds_{13} ds_{23}}. \tag{14}$$

The sum of the fit fractions for all components is not necessarily unity because of interference.

The amplitude analysis of B meson three-body decays reported here is performed by means of an unbinned maximum likelihood fit which minimizes the function

$$\mathcal{F} = -2 \sum_{\text{events}} \ln P(s_{13}, s_{23}; \xi), \tag{15}$$

where the function $P(s_{13}, s_{23}; \xi)$ describes the density of experimental events over the Dalitz plot; ξ is a vector of parameters.

An important question that arises in an unbinned analysis is the estimation of the goodness-of-fit. As the unbinned maximum likelihood fitting method does not provide a direct way to estimate the quality of the fit, we need a measure to assess how well any given fit represents the data. To do so the following procedure is applied. We first subdivide the entire Dalitz plot into $1\ (\mathrm{GeV}/c^2)^2 \times 1\ (\mathrm{GeV}/c^2)^2$ bins. If the number of events in the bin is smaller than $N_{\min} = 16$ it is combined with the adjacent bins until the number of events exceeds $N_{\min}$. After completing this procedure, the entire Dalitz plot is divided into a set of bins of varying size, and a χ^2 variable for the multinomial distribution can be calculated as

$$\chi^2 = -2 \sum_{i=1}^{N_{\text{bins}}} n_i \ln\left(\frac{p_i}{n_i}\right), \tag{16}$$

where n_i is the number of events observed in the i-th bin, and p_i is the number of predicted events from the fit. For a large number of events this formulation becomes equivalent to the usual one. Since we are minimizing the unbinned likelihood function, our "χ^2" variable does not asymptotically follow a χ^2 distribution but it is bounded by a χ^2 variable with $(N_{\text{bins}} - 1)$ degrees of freedom and a χ^2 variable with $(N_{\text{bins}} - k - 1)$ degrees of freedom [22], where k is the number of fit parameters. Because it is bounded by two χ^2 variables, it should be a useful statistic for comparing the relative goodness of fits for different models.

B. Efficiency, detector resolution and background

Several effects should be taken into account when fitting the experimental data. The reconstruction efficiency can vary significantly over the Dalitz-plot area and distort the initial distribution of signal events. In addition, there is also some fraction of background that fakes the signal. As is evident in Fig. 2, the background level in the signal region is comparable to that of the signal. Thus, understanding the distribution of background events over the Dalitz plot is important for an amplitude analysis. Finally, the detector resolution produces some smearing of the Dalitz-plot boundaries so that the phase space for the reconstructed B candidates exceeds the kinematically allowed area. To correct for this effect, three-body combinations are kinematically fit to the nominal B mass. As the intermediate resonances in general have large widths, we neglect the effect of detector resolution on the resonance shapes in most cases. In the case of narrow resonant states (for example, the ϕ meson in the $K^+K^+K^-$ final state or the χ_{c0} in both $K^+K^+K^-$ and $K^+\pi^+\pi^-$ final states), we take the detector resolution into account by convolving the signal probability density function with a two-dimensional Gaussian resolution function. The widths of the two-dimensional resolution function depend on the position in the Dalitz plot and are determined from the MC simulation.

To account for the background events and nonuniform reconstruction efficiency the event density function, $P(s_{13}, s_{23}; \xi)$ can be written as

$$P(s_{13}, s_{23}; \xi) = \frac{N_s \varepsilon(s_{13}, s_{23}) S(s_{13}, s_{23}, \xi) + n_b b(s_{13}, s_{23})}{N_s \int \varepsilon(s_{13}, s_{23}) S(s_{13}, s_{23}, \xi) ds_{13} ds_{23} + n_b}, \tag{17}$$

where N_s is the *initial* number of signal events distributed over the the Dalitz plot according to the signal density function $S(s_{13}, s_{23}, \xi)$, $\varepsilon(s_{13}, s_{23})$ is the reconstruction efficiency as a function of the position on the Dalitz plot, n_b is the expected number of the *observed* background events distributed with the density $b(s_{13}, s_{23})$, and a vector of parameters ξ (masses, widths and relative amplitudes and phases) is to be determined from the minimization. Equation (17) can be written in terms of the expected number of the observed signal events $n_s = N_s \varepsilon_s = N_s \int \varepsilon(s_{13}, s_{23}) S(s_{13}, s_{23}, \xi) ds_{13} ds_{23}$ and the background density function $B(s_{13}, s_{23}) = \varepsilon_b b(s_{13}, s_{23}) / \varepsilon(s_{13}, s_{23})$:

$$P(s_{13}, s_{23}, \xi) = \varepsilon(s_{13}, s_{23}) \times \frac{n_s S(s_{13}, s_{23}, \xi) \varepsilon_s + n_b B(s_{13}, s_{23}) / \varepsilon_b}{n_s + n_b}, \tag{18}$$

where the overall efficiencies ε_s and ε_b are determined from the MC simulation:

$$\begin{aligned} \varepsilon_s &= \int \varepsilon(s_{13}, s_{23}) S(s_{13}, s_{23}, \xi) ds_{13} ds_{23} \\ &= \frac{\Delta}{N_{\text{gen}}} \sum_{\text{MC}} S(s_{13}, s_{23}, \xi); \end{aligned} \tag{19}$$

$$\varepsilon_b = \int \varepsilon(s_{13}, s_{23}) B(s_{13}, s_{23}) ds_{13} ds_{23} = \frac{\Delta}{N_{\rm gen}} \sum_{\rm MC} B(s_{13}, s_{23}). \tag{20}$$

The sum $\sum_{\rm MC}$ is calculated from a set of MC events generated with a uniform distribution over the Dalitz plot, passed through the full detector simulation and subjected to all the event selection requirements; $N_{\rm gen}$ is the number of generated events; Δ is the Dalitz-plot area.

The likelihood function to be minimized can be written as

$$\mathcal{F} = -\sum_{\rm events} 2\ln\left(F \frac{S(s_{13}, s_{23}, \xi)}{\sum_{\rm MC} S(s_{13}^{\rm MC}, s_{23}^{\rm MC}, \xi)} + (1 - F) \times \frac{B(s_{13}, s_{23})}{\sum_{\rm MC} B(s_{13}^{\rm MC}, s_{23}^{\rm MC})}\right) - \sum_{\rm events} 2\ln\varepsilon(s_{13}, s_{23}) + \frac{(F - F_0)^2}{\sigma_{F_0}^2}, \tag{21}$$

where signal and background density functions are normalized to satisfy the requirement

$$\int S(s_{13}, s_{23}, \xi) ds_{13} ds_{23} = 1; \qquad \int B(s_{13}, s_{23}) ds_{13} ds_{23} = 1, \tag{22}$$

$F = n_s/(n_s + n_b)$ is the relative fraction of signal events in the data sample and F_0 is the estimated fraction from the fit to the ΔE distribution. The third term takes into account the uncertainty in our knowledge of the background contribution. As the second term in Eq. (21) does not depend on the fit parameters ξ, it is constant for a given set of experimental events and, thus, can be omitted. In Eq. (21) we assume there is no interference between signal and background processes. The background density function $B(s_{13}, s_{23})$ is determined from the unbinned likelihood fit to the experimental events in the $M_{\rm bc} - \Delta E$ sidebands.

C. Fitting the background shape

The definition of the $M_{\rm bc} - \Delta E$ sideband region is shown in Fig. 3. Figure 6 shows the Dalitz distributions for events in these sidebands; we find 7360 and 2176 events for the $K^+\pi^+\pi^-$ and $K^+K^+K^-$ final states, respectively. This is about 7 times the estimated number of background events in the corresponding signal region.

We use the following empirical parametrization to describe the distribution of background events over the Dalitz plot in the $K^+\pi^+\pi^-$ final state

$$B_{K\pi\pi}(s_{13}, s_{23}) = \alpha_1 e^{-\beta_1 s_{13}} + \alpha_2 e^{-\beta_2 s_{23}} + \alpha_3 e^{-\beta_3 s_{12}} + \alpha_4 e^{-\beta_4(s_{13} + s_{23})} + \alpha_5 e^{-\beta_5(s_{13} + s_{12})} + \alpha_6 e^{-\beta_6(s_{23} + s_{12})} + \gamma_1 |BW_1(K^*(892))|^2 + \gamma_2 |BW_1(\rho(770))|^2, \tag{23}$$

where $s_{13} \equiv M^2(K^+\pi^-)$, $s_{23} \equiv M^2(\pi^+\pi^-)$ and α_i ($\alpha_1 \equiv 1.0$), β_i, and γ_i are fit parameters. The first three terms in Eq. (23) are introduced to describe the background enhancement in the two-particle low invariant mass regions. This enhancement originates mainly from $e^+e^- \to q\bar{q}$ continuum events. Because of the jetlike structure of this background, all three particles in a three-body combination have almost collinear momenta. Hence, the invariant mass of at least one pair of particles is in the low mass region. In addition, it is often the case that two high momentum particles are combined with a low momentum particle to form a B candidate. In this case there are two pairs with low invariant masses and one pair with high invariant mass. This results in even stronger enhancement of the background in the corners of the Dalitz plot. This is taken into account by terms $4 - 6$ in Eq. (23). To account for the contribution from real $K^*(892)^0$ and $\rho(770)^0$ mesons, we introduce two more terms in Eq. (23), that are (noninterfer-

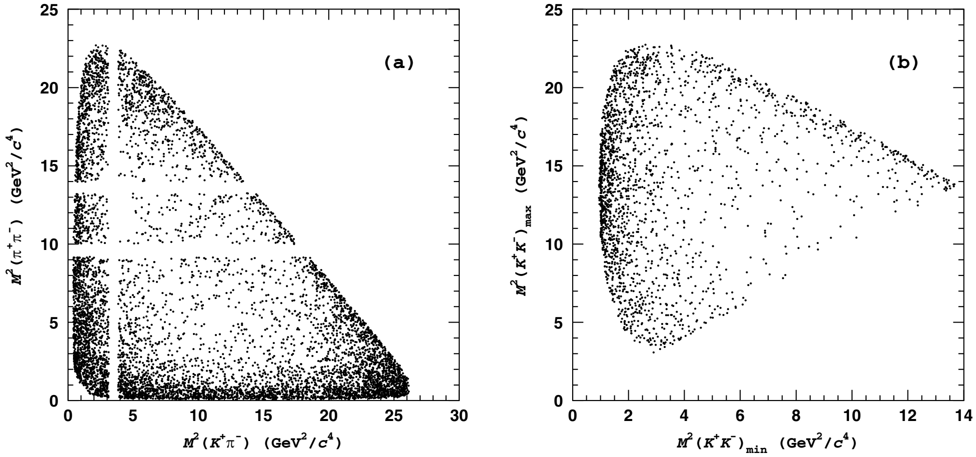

FIG. 6. Dalitz plots for events in the $\Delta E - M_{\rm bc}$ sidebands for the (a) $K^+\pi^+\pi^-$ and (b) $K^+K^+K^-$ (right) final states.

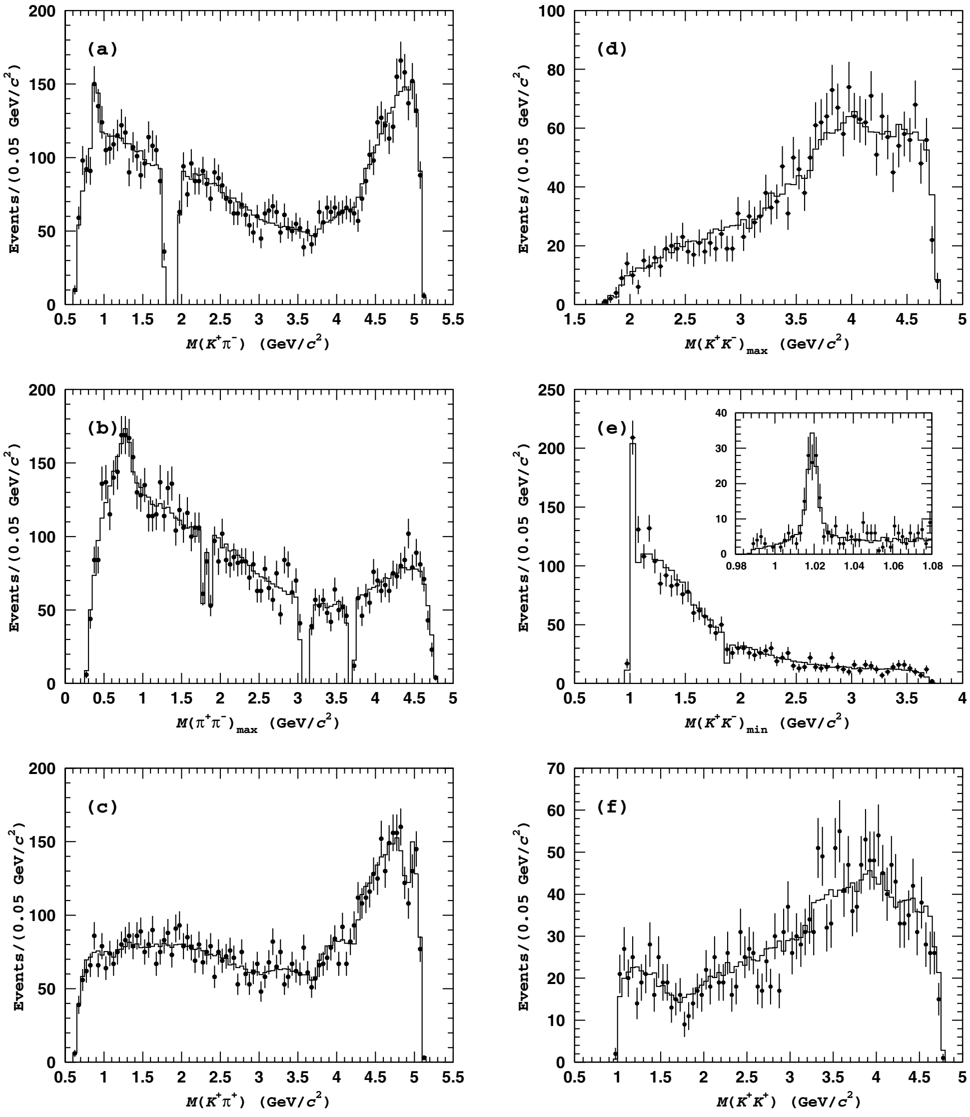

FIG. 7. Results of the best fit to the $K^+\pi^+\pi^-$ (left column) and $K^+K^+K^-$ (right column) events in the $\Delta E - M_{\rm bc}$ sidebands shown as projections onto two-particle invariant mass variables. Points with error bars are data; histograms are fit results. The inset in (e) shows the $\phi(1020)$ mass region in 2 MeV/c^2 bins.

ing) squared Breit-Wigner amplitudes [as in Eq. (5)], with masses and widths fixed at world average values [15]. For the $K^+K^+K^-$ final state the following, somewhat more complicated, parametrization is used

$$\begin{aligned} B_{KKK}(s_{13}, s_{23}) = {} & \alpha_1(1 - \alpha_2(s_{23} - \delta)^2)e^{-\beta_1(\sqrt{s_{13}} - \sqrt{s^0_{13}})} \\ & + \alpha_3(1 - \alpha_4(s_{23} - \delta)^2)e^{-\beta_3(\sqrt{s_{12}} - \sqrt{s^0_{12}})} \\ & + \alpha_5 e^{-\beta_5(\sqrt{s_{13}} + \sqrt{s_{12}})} \\ & + \alpha_6 e^{-\beta_6(\sqrt{s_{13}} + \sqrt{s_{23}})} \\ & + \gamma_1|BW_1(\phi)|^2, \end{aligned} \tag{24}$$

where $s_{13} \equiv \min\{M^2(K_1^+K^-), M^2(K_2^+K^-)\}$, $s_{23} \equiv \max\{M^2(K_1^+K^-), M^2(K_2^+K^-)\}$, $s_{12} \equiv M^2(K^+K^+)$ and s^0_{13} (s^0_{12}) is the minimal possible value (determined by phase space) for s_{13} (s_{12}), given the value of s_{23}.

The projections of the data and fits for the background events are shown in Fig. 7. The numerical values of the fit parameters are given in Table III. The $\chi^2/N_{\rm bins}$ values of the fits to the Dalitz plots are 213.7/195 for the $K^+\pi^+\pi^-$ and 57.6/66 for the $K^+K^+K^-$ final state, respectively.

D. Fitting the $B^+ \to K^+\pi^+\pi^-$ s signal

The Dalitz plot for $K^+\pi^+\pi^-$ events in the signal region is shown in Fig. 8(a). There are 2584 events in the signal region that satisfy all the selection requirements. In an attempt to describe all the features of the $K^+\pi^-$ and $\pi^+\pi^-$ mass spectra mentioned in Sec. V, we start with the following minimal matrix element for the

TABLE III. Parameters of the background density functions determined from the fit to events in the $M_{\rm bc} - \Delta E$ sidebands for the final states $K^+\pi^+\pi^-$ and $K^+K^+K^-$.

	$K^+\pi^+\pi^-$	$K^+K^+K^-$
α_1	1.0 (fixed)	1.0 (fixed)
α_2	0.78 ± 0.10	0.0131 ± 0.0017
α_3	1.22 ± 0.27	0.51 ± 0.10
α_4	1.51 ± 0.22	0.0118 ± 0.0031
α_5	2.05 ± 0.28	0.40 ± 0.17
α_6	1.98 ± 0.36	3.36 ± 1.13
β_1	1.25 ± 0.09	4.09 ± 0.32
β_2	1.66 ± 0.10	...
β_3	2.17 ± 0.23	4.83 ± 0.69
β_4	0.27 ± 0.01	...
β_5	0.38 ± 0.01	0.89 ± 0.13
β_6	0.27 ± 0.02	1.53 ± 0.16
γ_1	0.80 ± 0.23	2.80 ± 0.45
γ_2	2.25 ± 0.61	...
δ	...	14.21 ± 0.50

$B^+ \to K^+\pi^+\pi^-$ decay (referred to as model $K\pi\pi - A_J$):

$$\begin{aligned} S_{A_J}(K^+\pi^+\pi^-) = {} & a_{K^*}e^{i\delta_{K^*}}\mathcal{A}_1(\pi^+K^+\pi^-|K^*(892)^0) \\ & + a_{K_0^*}e^{i\delta_{K_0^*}}\mathcal{A}_0(\pi^+K^+\pi^-|K_0^*(1430)^0) \\ & + a_\rho e^{i\delta_\rho}\mathcal{A}_1(K^+\pi^+\pi^-|\rho(770)^0) \\ & + a_{f_0}e^{i\delta_{f0}}\mathcal{A}_0(K^+\pi^+\pi^-|f_0(980)) \\ & + a_{f_X}e^{i\delta_{fX}}\mathcal{A}_J(K^+\pi^+\pi^-|f_X) \\ & + a_{\chi_{c0}}e^{i\delta_{\chi c0}}\mathcal{A}_0(K^+\pi^+\pi^-|\chi_{c0}), \end{aligned} \qquad (25)$$

where the subscript J denotes the unknown spin of the $f_X(1300)$ resonance; amplitudes a_i, relative phases δ_i, masses and widths of the $f_0(980)$ and $f_X(1300)$ resonances are fit parameters. The masses and widths of all other resonances are fixed at their world average values [15]. While fitting the data, we choose the $K^*(892)^0\pi^+$ signal as our reference by fixing its amplitude and phase ($a_{K^*} \equiv 1$ and $\delta_{K^*} \equiv 0$). Figs. 9(a)–9(c) show the fit projections with model $K\pi\pi - A_0$ and the data [23]. The numerical values of the fit parameters in terms of relative phases and fractions calculated with Eq. (14) are given in Table IV. However, the data are not well represented by this matrix element, especially in the low $K^+\pi^-$ mass region as shown in Fig. 9(a). This is also demonstrated in Fig. 10, where the $K^+\pi^-$ invariant mass distributions are shown for the two $M^2(\pi^+\pi^-)$ regions: $M^2(\pi^+\pi^-) < 11\ \mathrm{GeV}/c^2$ and $M^2(\pi^+\pi^-) > 11\ \mathrm{GeV}/c^2$, which approximately correspond to the two helicity angle regions: $\cos\theta_H^{K\pi} < 0$ and $\cos\theta_H^{K\pi} > 0$, respectively. Result of the fit using model $K\pi\pi - A_0$ is shown as a dashed histogram in Fig. 10. (The helicity angle is defined as the angle between the direction of flight of the π^- in the $K^+\pi^-$ rest frame and the direction of $K^+\pi^-$ system in the B rest frame.) The difference in shape of the $M(K^+\pi^-)$ spectra clearly observed in Figs. 10(a) and 10(b) is consistent with what is expected in the case of interference of vector and scalar amplitudes. The scalar amplitude introduced by the $K_0^*(1430)^0$ state is found to be insufficient to reproduce this pattern. Thus, we modify the matrix element [Eq. (25)] by introducing an additional scalar amplitude. First, we construct model $K\pi\pi - B_J$, that is model $K\pi\pi - A_J$ with an additional scalar $K^+\pi^-$ resonance. A candidate for such a state could be the so-called κ resonance. An indication of the presence of the κ in $D^+ \to K^-\pi^+\pi^+$ decay with $M(\kappa) = 797 \pm 19 \pm 43\ \mathrm{MeV}/c^2$ and $\Gamma(\kappa) = 410 \pm 43 \pm 87\ \mathrm{MeV}/c^2$ was reported by the E791 Collaboration [24]. Results of the fit with model $K\pi\pi - B_0$ are summarized in Table IV. The agreement with the data is somewhat improved as compared to the model $K\pi\pi - A_0$. However, if the mass and the width of the κ are allowed to float, the fit finds $M(''\kappa'') = 1.23 \pm 0.07\ \mathrm{GeV}/c^2$ and $\Gamma(''\kappa'') = 2.41 \pm 0.26\ \mathrm{GeV}/c^2$. Both the mass and the width differ from those for the κ state measured by the E791

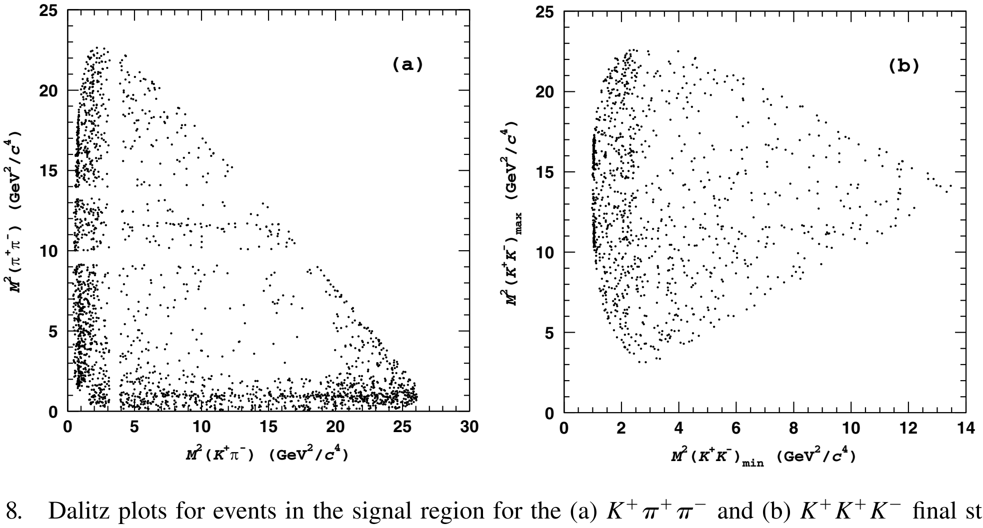

FIG. 8. Dalitz plots for events in the signal region for the (a) $K^+\pi^+\pi^-$ and (b) $K^+K^+K^-$ final states.

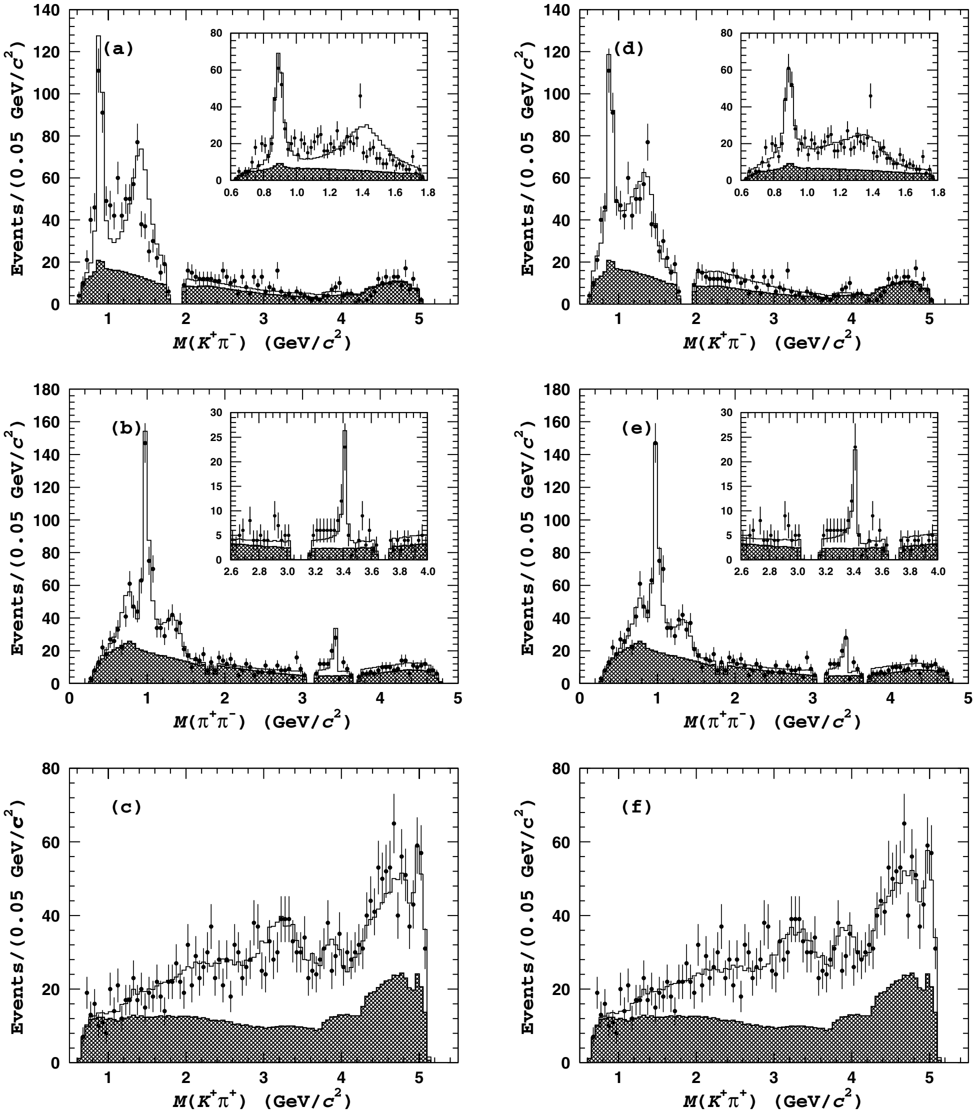

FIG. 9. Results of the fit to $K^+\pi^+\pi^-$ events in the signal region with model $K\pi\pi - \mathrm{A0}$ (left column) and model $K\pi\pi - C_0$ (right column). Points with error bars are data, the open histograms are the fit result and hatched histograms are the background components. Insets in (a) and (d) show the $K^*(892) - K_0^*(1430)$ mass region in 20 MeV/c^2 bins. Insets in (b) and (e) show the χ_{c0} mass region in 25 MeV/c^2 bins. Note that for plots (a) and (d) [(b) and (e)] an additional requirement $M(\pi^+\pi^-) > 1.5$ GeV/c^2 ($M(K^+\pi^-) > 1.5$ GeV/c^2) is imposed.

Collaboration. On the other hand, a scalar amplitude with such a large width could be an indication of the presence of a nonresonant amplitude. To check this hypothesis, we construct model $K\pi\pi - C_J$, that is model $K\pi\pi - A_J$ plus a nonresonant amplitude parametrized by Eq. (11). Results of the fit with model $K\pi\pi - C_0$ are given in Table IV and shown in Figs. 9(d)–9(f).

The mass and width of the $f_X(1300)$ state obtained from the fit with model $K\pi\pi - C_0$ are consistent with those for the $f_0(1370)$ [15]. If a tensor amplitude is used for the $f_X(1300)$ state (model $K\pi\pi - C_2$), the fit finds $M(f_X(1300)) = 1.377 \pm 0.038$ GeV/c^2 and $\Gamma(f_X(1300)) = 0.085 \pm 0.031$ GeV/c^2 ($-2\log\mathcal{L} = -4013.0$; $\chi^2/N_{\rm bin} = 103.8/106$), which disagree with the world average $f_2(1270)$ parameters [15]. In the case of a vector amplitude (model $K\pi\pi - C_1$), the fit gives $M(f_X(1300)) = 1.330 \pm 0.019$ GeV/c^2 and $\Gamma(f_X(1300)) = 0.210 \pm 0.048$ GeV/c^2 ($-2\log\mathcal{L} = -4048.1$; $\chi^2/N_{\rm bin} = 105.5/106$). Based on this study, we choose model $K\pi\pi - C_0$ as our default and obtain all the final results for the $B^+ \to K^+\pi^+\pi^-$ decay using this model. Figure 11 shows the $M(K^+\pi^-)$ ($M(\pi^+\pi^-)$) distributions in slices of $M^2(\pi^+\pi^-)$ ($M^2(K^+\pi^-)$) to allow a more detailed comparison of the data and fit results with model $K\pi\pi - C_0$.

In addition to the two-particle invariant mass distributions shown in Figs. 9 and 11, the helicity angle distributions for several regions are shown in Fig. 12. (For the

TABLE IV. Summary of fit results to $K^+\pi^+\pi^-$ events in the signal region. The two values given for model $K\pi\pi - C_0$ correspond to two solutions (see text for details).

Parameter		Model $K\pi\pi - A_0$	$K\pi\pi - B_0$	$K\pi\pi - C_0$ Solution 1/Solution 2
$K^*(892)^0\pi^+$	Fraction, %	18.0 ± 1.4	14.1 ± 1.3	$13.7 \pm 1.1/12.6 \pm 1.3$
	Phase, °	0 (fixed)		
$K_0^*(1430)^0\pi^+$	Fraction, %	42.1 ± 3.7	48.6 ± 3.4	$58.4 \pm 2.7/10.7 \pm 2.8$
	Phase, °	11 ± 8	73 ± 9	$36 \pm 7/-11 \pm 9$
$\rho(770)^0K^+$	Fraction, %	11.2 ± 1.4	9.85 ± 1.20	$10.0 \pm 1.5/8.18 \pm 0.92$
	Phase, °	-17 ± 18	25 ± 25	$-52 \pm 18/47 \pm 25$
$f_0(980)K^+$	Fraction, %	16.5 ± 1.5	17.4 ± 1.7	$15.8 \pm 2.5/14.0 \pm 1.4$
	Phase, °	33 ± 19	74 ± 23	$20 \pm 16/94 \pm 17$
	Mass, GeV/c^2	0.975 ± 0.004	0.976 ± 0.004	$0.976 \pm 0.004/0.975 \pm 0.003$
	Width, GeV/c^2	0.063 ± 0.009	0.065 ± 0.009	$0.061 \pm 0.009/0.053 \pm 0.009$
$\chi_{c0}K^+$	Fraction, %	3.56 ± 0.93	3.09 ± 0.87	$2.86 \pm 0.58/2.13 \pm 0.67$
	Phase, °	-124 ± 16	-37 ± 24	$-29 \pm 23/-15 \pm 22$
$f_X(1300)K^+$	Fraction, %	6.70 ± 1.42	6.14 ± 1.50	$5.47 \pm 2.47/3.75 \pm 1.70$
	Phase, °	160 ± 18	185 ± 21	$158 \pm 18/-134 \pm 22$
	Mass, GeV/c^2	1.369 ± 0.026	1.344 ± 0.026	$1.369 \pm 0.026/1.400 \pm 0.028$
	Width, GeV/c^2	0.220 ± 0.063	0.227 ± 0.070	$0.185 \pm 0.052/0.165 \pm 0.048$
$\kappa\pi^+$	Fraction, %	...	20.3 ± 0.0	...
	Phase, °	...	-139 ± 6	...
	Mass, GeV/c^2	...	0.797 (fixed)	...
	Width, GeV/c^2	...	0.410 (fixed)	...
Nonresonant	Fraction, %	...	...	$36.2 \pm 3.2/40.1 \pm 5.2$
	$a_2^{\text{nr}}/a_1^{\text{nr}}$	...	...	$0.34 \pm 0.09/0.42 \pm 0.09$
	δ_1^{nr}, °	...	...	$-25 \pm 7/8 \pm 8$
	δ_2^{nr}, °	...	...	$140 \pm 16/-146 \pm 13$
	α	...	...	$0.102 \pm 0.023/0.106 \pm 0.022$
Charmless total[a]				
	Fraction, %	97.7 ± 0.6	96.6 ± 0.8	$97.5 \pm 0.7/97.6 \pm 0.6$
$-2\ln\mathcal{L}$		-3845.3	-3966.6	$-4041.8/-4024.4$
χ^2		227.8	129.0	104.2/107.1
N_{bins}		106	106	106
$N_{\text{fit.var.}}$		14	16	19

[a] Here "Charmless total" refers to the total three-body $B^+ \to K^+\pi^+\pi^-$ signal excluding the contribution from $B^+ \to \chi_{c0}K^+$.

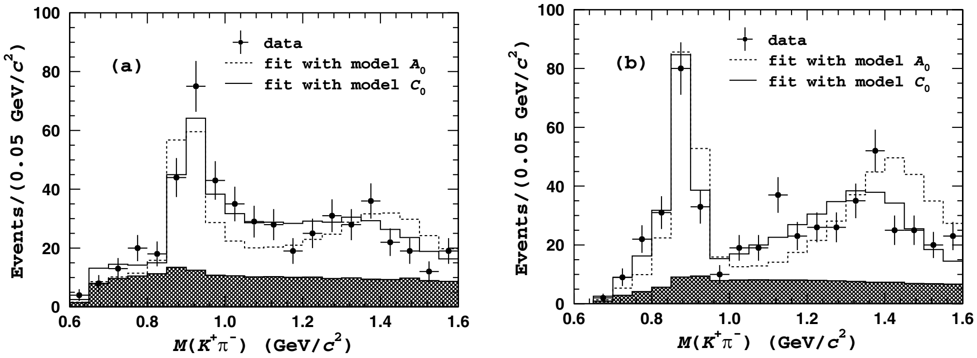

FIG. 10. $K^+\pi^-$ invariant mass distributions for $K^+\pi^+\pi^-$ events with (a) $M^2(\pi^+\pi^-) < 11$ GeV/c^2 and (b) $M^2(\pi^+\pi^-) > 11$ GeV/c^2.

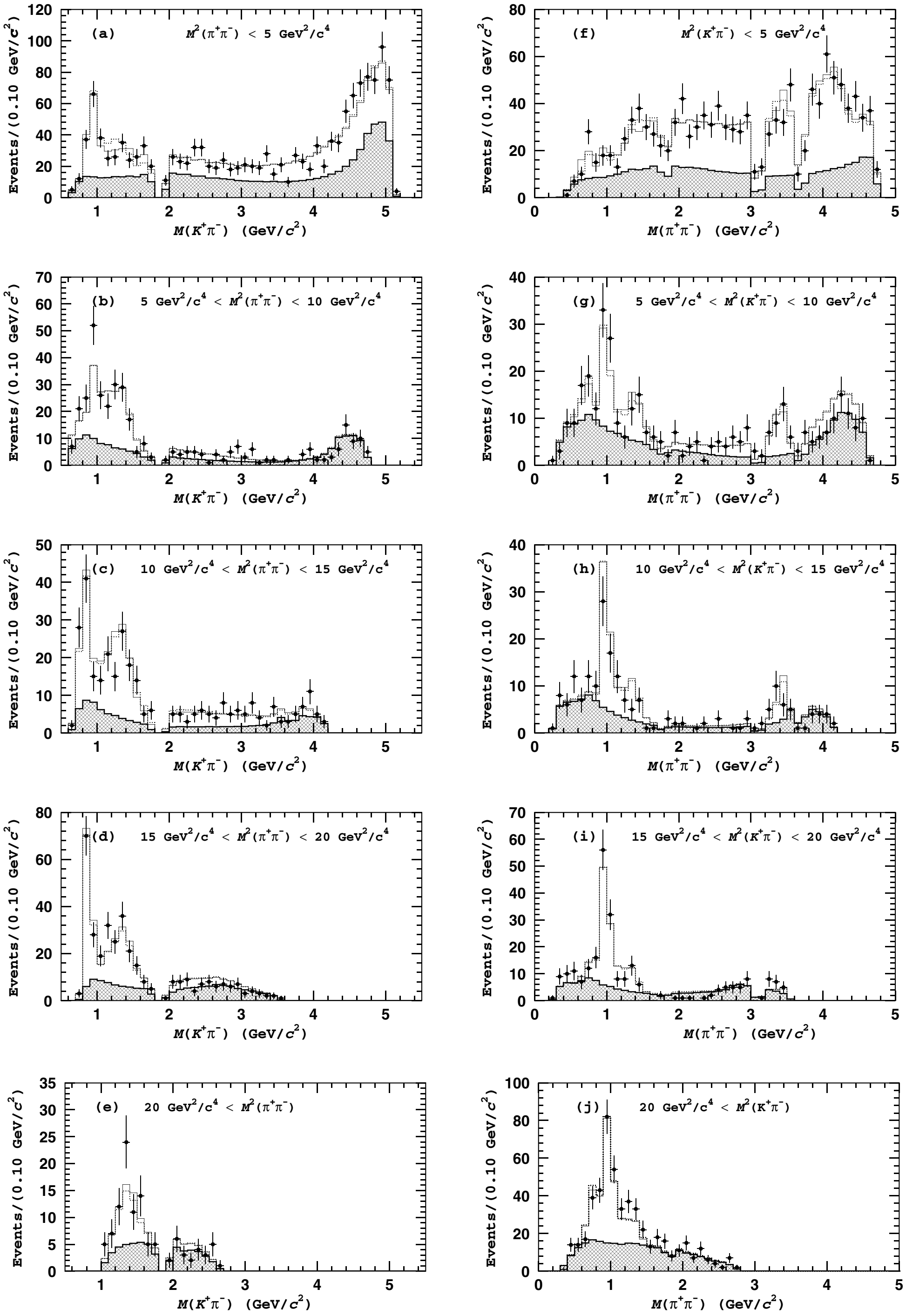

FIG. 11. $M(K^+\pi^-)$ ($M(\pi^+\pi^-)$) distributions in slices of $M(\pi^+\pi^-)$ ($M(K^+\pi^-)$). Points with error bars are data, the open histograms are the fit results with model $K\pi\pi - C_0$ and the hatched histogram is the background component. Solid and dotted histograms correspond to Solution 1 and Solution 2, respectively, (see Table IV and text for details).

$\pi^+\pi^-$ combination the helicity angle is defined in a similar way as for $K^+\pi^-$ combination.) All plots shown in Fig. 12 demonstrate good agreement between data and the fit.

To test for the contribution of other possible quasi-two-body intermediate states such as $K^*(1410)^0\pi^+$, $K^*(1680)^0\pi^+$, $K_2^*(1430)^0\pi^+$, or $f_2(1270)K^+$, we include an additional amplitude of each of these channels in model $K\pi\pi - C_0$ and repeat the fit to data. None of these channels have a statistically significant signal.

To estimate the model dependent uncertainty in the branching fractions for individual quasi-two-body chan-

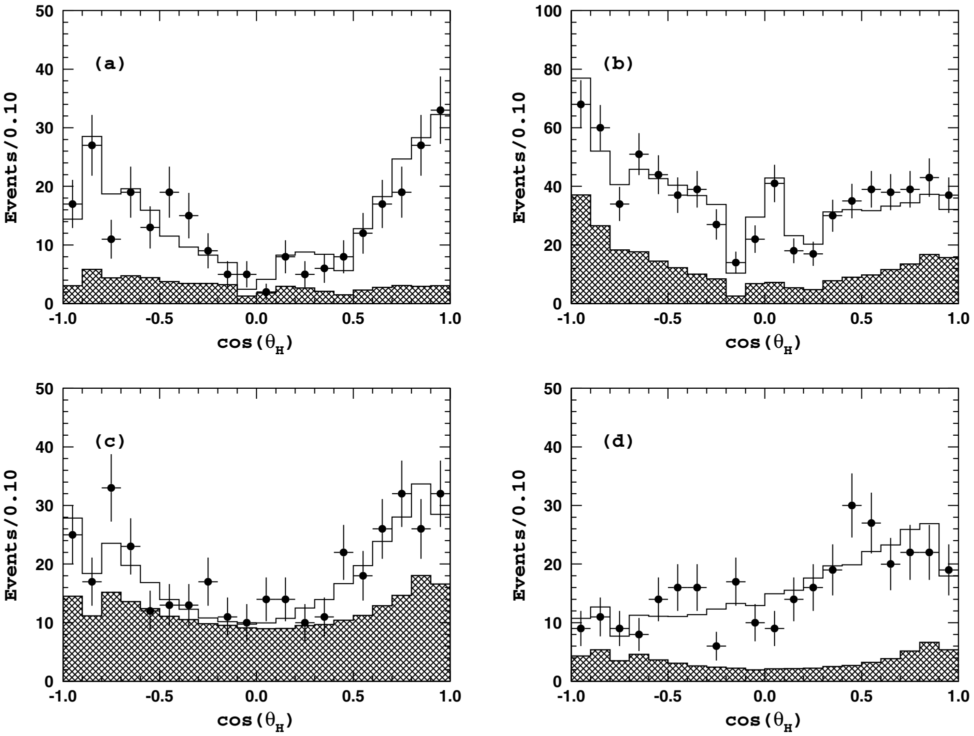

FIG. 12. Helicity angle distributions for $K^+\pi^+\pi^-$ events in different regions: (a) $K^*(892)^0$ ($0.82\ \mathrm{GeV}/c^2 < M(K^+\pi^-) < 0.97\ \mathrm{GeV}/c^2$); (b) $K_0^*(1430)^0$ ($1.0\ \mathrm{GeV}/c^2 < M(K^+\pi^-) < 1.76\ \mathrm{GeV}/c^2$); (c) $\rho(770)^0$ ($M(\pi^+\pi^-) < 0.90\ \mathrm{GeV}/c^2$) and (d) $f_0(980)$ ($0.90\ \mathrm{GeV}/c^2 < M(\pi^+\pi^-) < 1.06\ \mathrm{GeV}/c^2$). Points with error bars are data, the open histogram is the fit result with model $K\pi\pi - C_0$ and the hatched histogram is the background component. Visible irregularities are due to vetoes applied on invariant masses of two-particle combinations.

nels, we use the results of fits obtained with models $K\pi\pi - B_J$ and $K\pi\pi - C_J + R$, where R is one of an additional resonances mentioned above. We also use different parametrizations of the nonresonant amplitude to estimate the related uncertainty. We try the following alternative parametrizations:

(a) $\mathcal{A}_{\mathrm{nr}}(K^+\pi^+\pi^-) = a_1^{\mathrm{nr}} e^{-\alpha s_{13}} e^{i\delta_1^{\mathrm{nr}}} + a_2^{\mathrm{nr}} e^{-\alpha s_{23}} e^{i\delta_2^{\mathrm{nr}}} + a_3^{\mathrm{nr}} e^{-\alpha s_{12}} e^{i\delta_3^{\mathrm{nr}}}$;

(b) $\mathcal{A}_{\mathrm{nr}}(K^+\pi^+\pi^-) = \frac{a_1^{\mathrm{nr}}}{s_{13}} e^{i\delta_1^{\mathrm{nr}}} + \frac{a_2^{\mathrm{nr}}}{s_{23}} e^{i\delta_2^{\mathrm{nr}}}$;

(c) $\mathcal{A}_{\mathrm{nr}}(K^+\pi^+\pi^-) = a^{\mathrm{nr}} e^{i\delta^{\mathrm{nr}}}$.

While fitting the data with model $K\pi\pi - C_0$, we found that two solutions with very similar likelihood values exist. The comparison between the two solutions and the data are shown in Fig. 11. The main difference between these two solutions is the relative fractions of the total $B^+ \to K^+\pi^+\pi^-$ signal ascribed to the $B^+ \to K_0^*(1430)^0\pi^+$ decay: the fraction of this channel changes by a factor of about five. The reason for the existence of the second solution is similar behavior of the two amplitudes [the nonresonant component parametrized by Eq. (11) and the scalar $K_0^*(1430)^0\pi^+$ amplitude] as functions of $M^2(K^+\pi^-)$. Because of the large width of the $K_0^*(1430)^0$ resonance, these two amplitudes can be, to a large extent, interchanged providing a nearly identical description of the data. An even stronger effect is observed in the case of model $K\pi\pi - B_0$ when the mass and width of the "κ" resonance is allowed to float. In this case the two amplitudes are almost identical. A similar behavior is observed for all the parametrizations used to describe the nonresonant amplitude. The existence of secondary maxima of the likelihood function is confirmed with MC simulation (see Sec. VIII for the more detailed discussion).

E. Fitting the $B^+ \to K^+K^+K^-$ signal

The Dalitz plot for $K^+K^+K^-$ events in the signal region is shown in Fig. 8(b). There are 1400 events in the signal region. In the analysis of the $K^+K^+K^-$ final state we follow the same strategy as in the case of the $K^+\pi^+\pi^-$ state. In an attempt to describe all the features in the K^+K^- mass spectrum mentioned in Sec. V, we start with the following minimal matrix element of the $B^+ \to K^+K^+K^-$ decay (referred to as model $KKK - A_J$):

$$\begin{aligned} S_A(K^+K^+K^-) = {} & a_\phi e^{i\delta_\phi}(\mathcal{A}_1(K_1^+K_2^+K^-|\phi) \\ & + \mathcal{A}_1(K_2^+K_1^+K^-|\phi)) \\ & + a_{\chi_{c0}} e^{i\delta_{\chi_{c0}}}(\mathcal{A}_0(K_1^+K_2^+K^-|\chi_{c0}) \\ & + \mathcal{A}_0(K_2^+K_1^+K^-|\chi_{c0})) \\ & + a_{f_X} e^{i\delta_{f_X}}(\mathcal{A}_J(K_1^+K_2^+K^-|f_X) \\ & + \mathcal{A}_J(K_2^+K_1^+K^-|f_X)), \end{aligned} \tag{26}$$

where the subscript J denotes the unknown spin of the $f_X(1500)$ resonance; amplitudes a_i, relative phases δ_i, mass and width of the $f_X(1500)$ resonance are fit parameters. As there are two identical kaons in the final state, the amplitude in Eq. (26) is symmetrized with respect to $K_1^+ \leftrightarrow K_2^+$ interchange. When fitting the data, we choose the $f_X(1500)K^+$ signal as our reference by fixing its amplitude and phase ($a_{f_X} \equiv 1$ and $\delta_{f_X} \equiv 0$). Figs. 13(a)–13(c) show the two-kaon invariant mass projections for model $KKK - A_0$ and the data. The numerical values of the fit parameters are given in Table V. Although the data are described relatively well even with this simple matrix element, there is a region where the agreement is not satisfactory. The enhancement of signal events in the higher K^+K^- mass range visible in Fig. 13(a) causes the width of the $f_X(1500)$ state determined from the fit with model $KKK - A_0$ to be very large. This results in a poor description of the data in the $M(K^+K^-) \simeq 1.5$ GeV/c^2 region, where the peaking structure is significantly narrower. On the other hand, as for $B^+ \to K^+\pi^+\pi^-$, the excess of signal events at high $M(K^+K^-)$ may be evidence for nonresonant $B^+ \to K^+K^+K^-$ decay. To test this hypothesis, we extend model $KKK - A_J$ to include a nonresonant amplitude (model $KKK - B_J$) parametrized by Eq. (12). Results of the fit with model $KKK - B_0$ are shown in Figs. 13(d)–13(f); numerical values of the fit parameters are given in Table V. The agreement with data is significantly improved compared to model $KKK - A_0$.

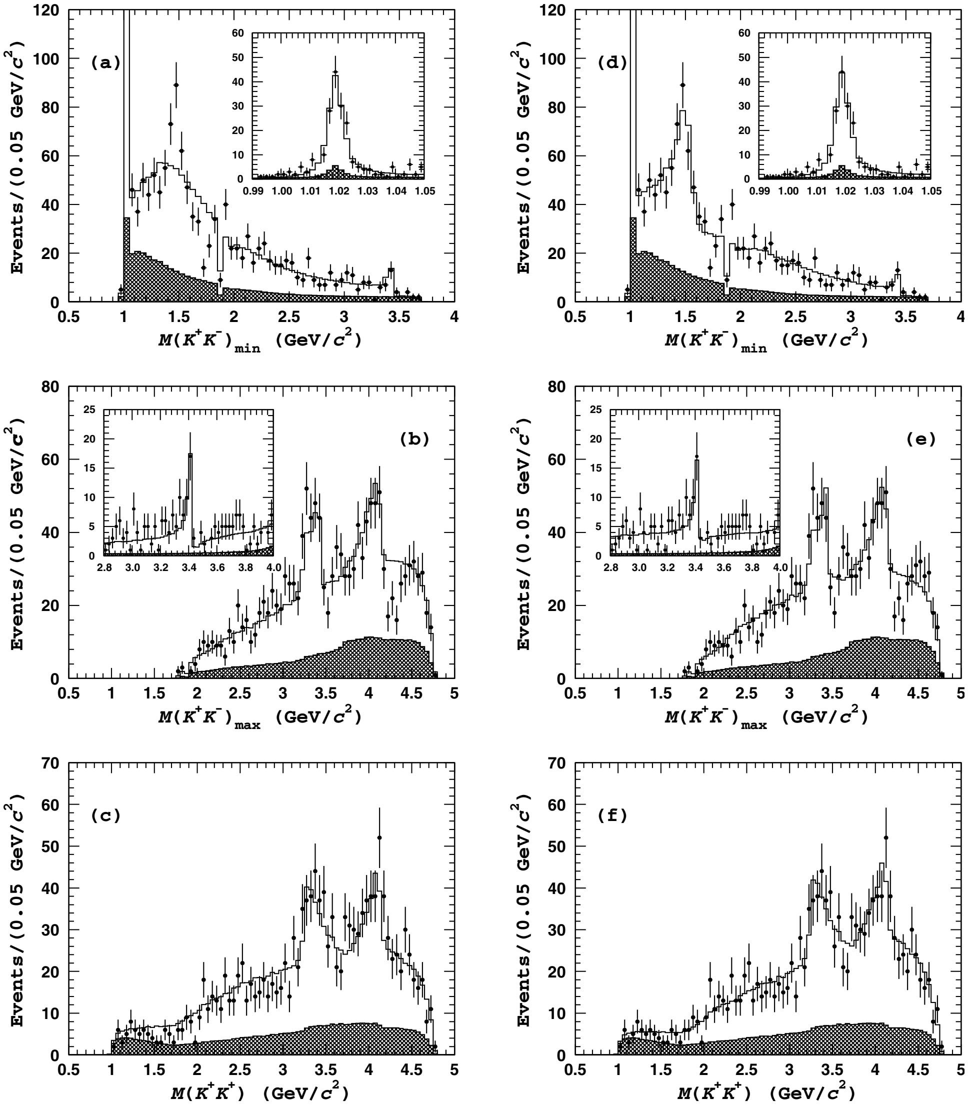

FIG. 13. Results of the fit with the model $KKK - A_0$ (left column) and $KKK - B_0$ (right column) to events in the signal region. Note that the first and the second rows show the distributions for the $M(K^+K^-)_{\mathrm{min}}$ and $M(K^+K^-)_{\mathrm{max}}$, respectively. Points with error bars are data, the open histogram is the fit result and hatched histogram is the background component. Insets in (a) and (d) show the $\phi(1020)$ mass region in 2 MeV/c^2 bins. Insets in (b) and (e) show the χ_{c0} mass region in 25 MeV/c^2 bins with an additional requirement 2.0 GeV/c^2 $< M(K^+K^-)_{\mathrm{min}} <$ 3.4 GeV/c^2.

TABLE V. Summary of fit results to $K^+K^+K^-$ events in the signal region. The two values given for model $KKK - B_0$ correspond to the two solutions (see text for details).

Parameter		Model	
		$KKK - A_0$	$KKK - B_0$ Solution 1/Solution 2
$\phi(1020)K^+$	Fraction, %	14.0 ± 1.2	$14.7 \pm 1.3/15.2 \pm 1.3$
	Phase, °	-17 ± 11	$-123 \pm 10/-200 \pm 10$
$f_X(1500)K^+$	Fraction, %	83.3 ± 2.5	$63.4 \pm 6.9/8.21 \pm 1.94$
	Phase, °	0 (fixed)	
	Mass, GeV/c^2	1.373 ± 0.025	$1.524 \pm 0.014/1.491 \pm 0.018$
	Width, GeV/c^2	0.720 ± 0.058	$0.136 \pm 0.023/0.145 \pm 0.029$
$\chi_{c0}K^+$	Fraction, %	4.48 ± 1.4	$2.67 \pm 0.82/8.01 \pm 1.35$
	Phase, °	165 ± 15	$-118 \pm 15/127 \pm 10$
Nonresonant	Fraction, %	…	$74.8 \pm 3.6/65.1 \pm 5.1$
	Phase, °	…	$-68 \pm 9/61 \pm 10$
	α	…	$0.121 \pm 0.014/0.116 \pm 0.015$
Charmless total[a]			
	Fraction, %	96.0 ± 0.7	$95.2 \pm 1.0/95.6 \pm 0.9$
$-2\ln\mathcal{L}$		-2140.4	$-2218.2/-2177.4$
χ^2		65.0	43.3/57.1
N_{bins}		53	53
$N_{\text{fit.var.}}$		6	9

[a] Here "Charmless total" refers to the total three-body $B^+ \to K^+K^+K^-$ signal excluding the contribution from $B^+ \to \chi_{c0}K^+$.

In order to check the sensitivity of the data to the spin of the $f_X(1500)$ state, we replace the scalar amplitude by a vector (model $KKK - B_1$) or a tensor (model $KKK - B_2$) amplitude for the $f_X(1500)$ with its mass and width as free parameters. The scalar hypothesis gives the best fit. Figure 14 shows a detailed comparison of the fit and the $M(K^+K^-)_{\min}$ ($M(K^+K^-)_{\max}$) distributions for different slices of $M^2(K^+K^-)_{\max}$ ($M^2(K^+K^-)_{\min}$). Finally, Fig. 15 shows the helicity angle distributions for the ϕ and $f_X(1500)$ regions. Based on these results, we choose model $KKK - B_0$ as the default. All of the final results for the decay $B^+ \to K^+K^+K^-$ are based on this model.

To estimate the model dependent uncertainty in the relative fractions of individual quasi-two-body intermediate states and determine the contribution of other possible quasi-two-body intermediate states, we modify model $KKK - B_0$ to include an additional decay channel and repeat the fit to the data. In particular we test the $\phi(1680)K^+$, $f_2'(1525)K^+$ and $a_2(1320)K^+$ channels. In all cases the fit finds no statistically significant signal for the newly added channel. Since we observe a clear $f_0(980)K^+$ signal in the $K^+\pi^+\pi^-$ final state, we try to include the $f_0(980)K^+$ amplitude in the $B^+ \to K^+K^+K^-$ matrix element as well: no statistically significant contribution from this channel is found. As the dominant model uncertainty is related to the parametrization of the nonresonant amplitude, we use several alternative, yet also arbitrary, parametrizations to estimate the relevant uncertainty:

(a) $\mathcal{A}_{\text{nr}}(K^+K^+K^-) = a_1^{\text{nr}}(e^{-\alpha s_{13}} + e^{-\alpha s_{23}})e^{i\delta_1^{\text{nr}}} + a_2^{\text{nr}}e^{-\alpha s_{12}}e^{i\delta_2^{\text{nr}}}$;

(b) $\mathcal{A}_{\text{nr}}(K^+K^+K^-) = a_1^{\text{nr}}(\frac{1}{s_{13}} + \frac{1}{s_{23}})e^{i\delta_1^{\text{nr}}}$;

(c) $\mathcal{A}_{\text{nr}}(K^+K^+K^-) = a^{\text{nr}}e^{i\delta^{\text{nr}}}$.

As in the case of $B^+ \to K^+\pi^+\pi^-$, we find two solutions in the fit to $K^+K^+K^-$ events with model $KKK - B_0$. The comparison between the two solutions and the data are shown in Fig. 14. The main difference in these two solutions is in the fraction of the $B^+ \to f_X(1500)K^+$ signal which changes by about an order of magnitude. Results for both solutions of the $KKK - B_0$ model are given in Table V.

F. MC pseudoexperiments

The parameters that are directly determined from the fit to data are the amplitudes and phases with their statistical errors. However, while the relative fraction for a particular quasi-two-body channel depends only on the corresponding amplitude in the matrix element, its statistical error depends on the statistical errors of all amplitudes and phases. To determine the statistical errors for quasi-two-body channels, we use a MC pseudoexperiment technique.

MC pseudoexperiments are MC generated samples which are the proper mixture of "signal" and "background" events distributed according to density functions determined from the fit to experimental events. For each model we generate 100 statistically independent MC pseudoexperiments with numbers of signal and background

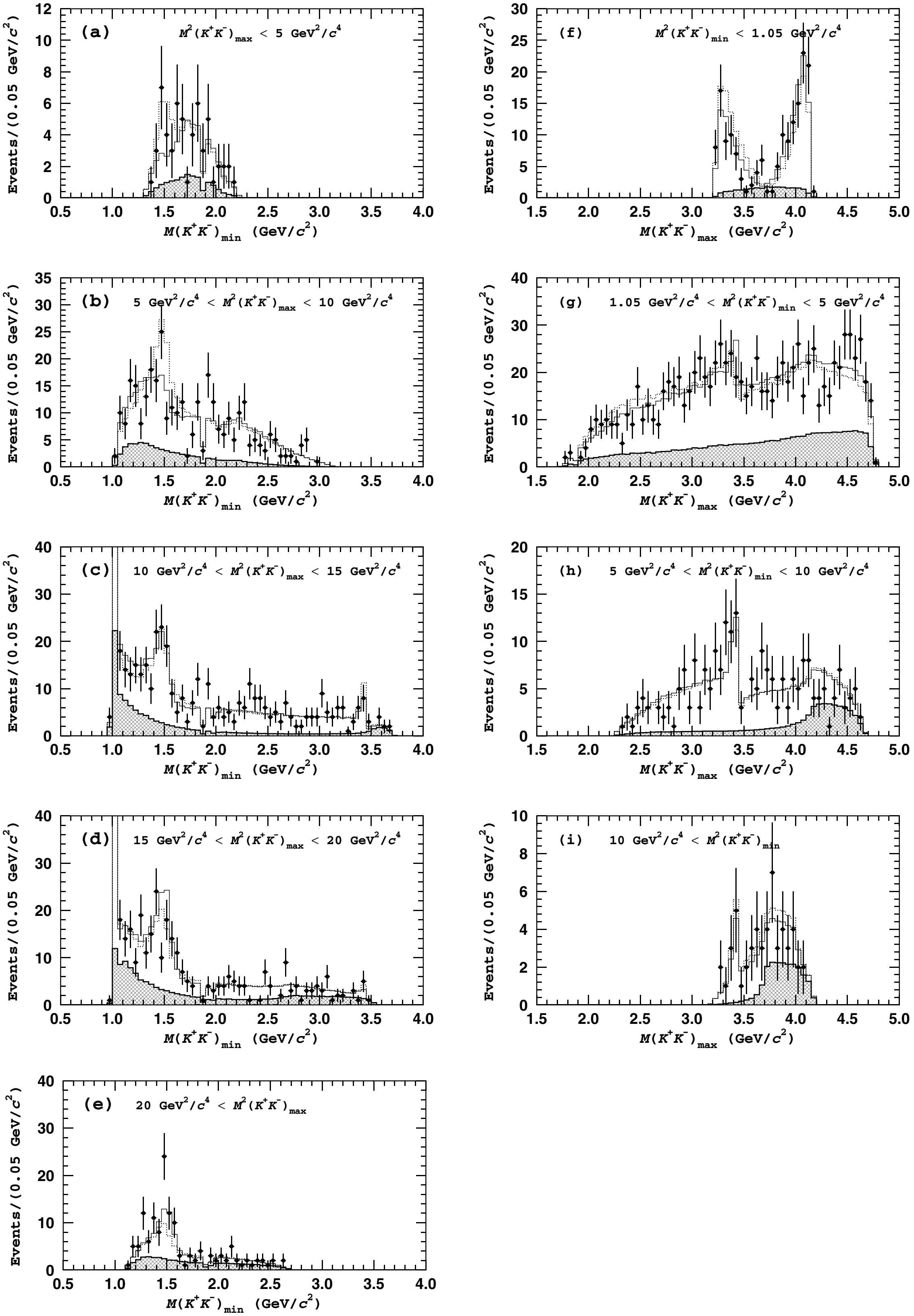

FIG. 14. $M(K^+K^-)_{\rm min}$ ($M(K^+K^-)_{\rm max}$) distributions in slices of $M(K^+K^-)_{\rm max}$ ($M(K^+K^-)_{\rm min}$). Points with error bars are data, the open histograms are the fit results with model $KKK - B_0$ and the hatched histogram is the background component. Solid and dotted histograms correspond to Solution 1 and Solution 2, respectively, (see Table V and text for details).

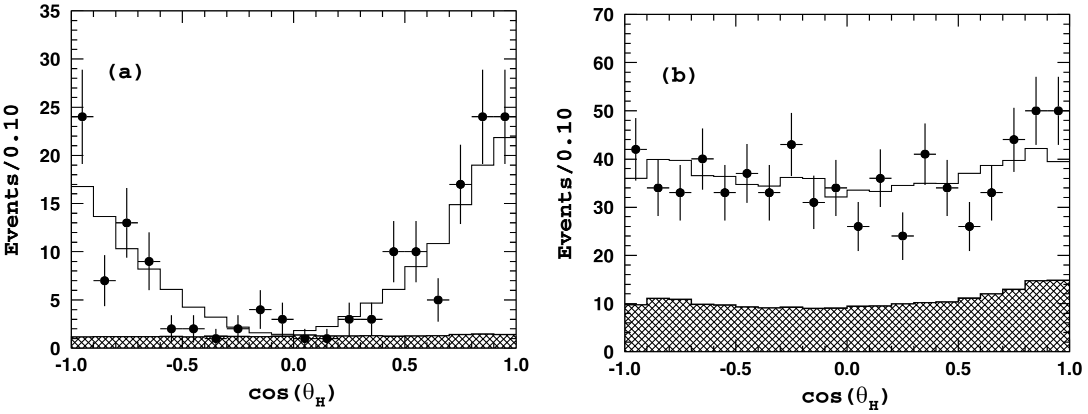

FIG. 15. Helicity angle distributions for events in the (a) ϕ mass region ($(M(K^+K^-)_{\rm min} < 1.05~{\rm GeV}/c^2)$) and in the (b) $f_X(1500)$ region ($1.05~{\rm GeV}/c^2 < M(K^+K^-)_{\rm min} < 3.0~{\rm GeV}/c^2$). Points with error bars are data, the open histogram is the fit result with model $KKK - B_0$ and the hatched histogram is the background component.

events equal to those found in the experiment, fit these MC samples, and determine the relative fractions f_l of quasi-two-body channels for each sample. The f_l distributions are then fit by a Gaussian function; the sigma of the Gaussian determined from the fit is assigned as the statistical error.

VII. BRANCHING FRACTION RESULTS AND SYSTEMATIC UNCERTAINTIES

In previous sections we determined the relative fractions of various quasi-two-body intermediate states in three-body $B^+ \to K^+\pi^+\pi^-$ and $B^+ \to K^+K^+K^-$ decays. To translate those values into absolute branching fractions, we first need to determine the branching fractions for the three-body decays. To determine the reconstruction efficiency for the $B^+ \to K^+\pi^+\pi^-$ and $B^+ \to K^+K^+K^-$ decays, we use a MC simulation where events are distributed over phase space according to the matrix elements of model $K\pi\pi - C_0$ and model $KKK - B_0$, respectively. The corresponding reconstruction efficiencies are $21.1 \pm 0.2\%$ and $22.3 \pm 0.2\%$. Results of the branching fraction calculations for the total three-body charmless $B^+ \to K^+\pi^+\pi^-$ and $B^+ \to K^+K^+K^-$ decays [25] and all the quasi-two-body intermediate channels are summarized in Table VI, where the first quoted error is statistical, the second is systematic and the third is the model uncertainty. Branching fractions for $R \to h^+h^-$ decays are taken from [15].

For most of the quasi-two-body channels the difference in branching fractions from the two solutions is relatively small and treated as model error. However values for the $B^+ \to K_0^*(1430)^0\pi^+$ branching fraction are substantially different for the two solutions and we quote both values in Table VI. For the $B^+ \to \chi_{c0}K^+$ decay the central value is calculated by combining measurements in $\chi_{c0} \to \pi^+\pi^-$ channel and the best fit in $\chi_{c0} \to K^+K^-$ channel, the second solution in $\chi_{c0} \to K^+K^-$ channel is used for model error estimation. As the interpretation of the $f_X(1300)$ and $f_X(1500)$ states is uncertain, we do not quote the corresponding branching fractions.

For quasi-two-body channels where no significant signal is observed, we calculate 90% confidence level upper limits f_{90} for their fractions. To determine the upper limit we use the following formula

$$0.90 = \frac{\int_0^{f_{90}} G(a, \sigma; x)dx}{\int_0^{\infty} G(a, \sigma; x)dx}, \tag{27}$$

where $G(a, \sigma; x)$ is a Gaussian function with the measured mean value a for the signal fraction and its statistical error σ. To account for the model uncertainty we determine the resonance's contribution with different parameterizations of the nonresonant amplitude and use the largest value to evaluate the upper limit. To account for the systematic uncertainty we decrease the reconstruction efficiency by 1 standard deviation.

The dominant sources of systematic error are listed in Table VII. For the branching fractions of three-body $B^+ \to K^+\pi^+\pi^-$ and $B^+ \to K^+K^+K^-$ decays, we estimate the systematic uncertainty due to variations of the reconstruction efficiency over the Dalitz plot by varying the relative phases and amplitudes of the quasi-two-body states within their errors. The systematic uncertainty due to requirements on event shape variables is estimated from a comparison of their distributions for signal MC events and $B^+ \to \bar{D}^0\pi^+$ events in the data. We estimate the uncertainty in the signal yield extraction from the fit to the ΔE distribution by varying the parameters of the fitting function within their errors. The uncertainty due to background parametrization is estimated by varying the relative fraction of the $B\bar{B}$ background component and the slope of the $q\bar{q}$ background function within their errors. The uncertainty from the particle identification efficiency is esti-

TABLE VI. Summary of branching fraction results. The first quoted error is statistical, the second is systematic and the third is the model error. The branching fraction values in this table are obtained from the product of the appropriate fractions in Tables IV and V with the branching ratios obtained from the signal yields in Table I. Note that the yields in Table I include χ_{c0} contributions. The charmless total fractions in this table exclude the χ_{c0} contribution. The value given in brackets for the $K_0^*(1430)^0\pi^+$ channel corresponds to the second solution (see text for details).

Mode	$\mathcal{B}(B^+ \to Rh^+) \times \mathcal{B}(R \to h^+h^-) \times 10^6$	$\mathcal{B}(B^+ \to Rh^+) \times 10^6$
$K^+\pi^+\pi^-$ Charmless total	…	$46.6 \pm 2.1 \pm 4.3$
$K^*(892)^0\pi^+$, $K^*(892)^0 \to K^+\pi^-$	$6.55 \pm 0.60 \pm 0.60^{+0.38}_{-0.57}$	$9.83 \pm 0.90 \pm 0.90^{+0.57}_{-0.86}$
$K_0^*(1430)^0\pi^+$, $K_0^*(1430)^0 \to K^+\pi^-$	$27.9 \pm 1.8 \pm 2.6^{+8.5}_{-5.4}$	$45.0 \pm 2.9 \pm 6.2^{+13.7}_{-8.7}$
	$(5.12 \pm 1.36 \pm 0.49^{+1.91}_{-0.51})$	$(8.26 \pm 2.20 \pm 1.19^{+3.08}_{-0.82})$
$K^*(1410)^0\pi^+$, $K^*(1410)^0 \to K^+\pi^-$	<2.0	…
$K^*(1680)^0\pi^+$, $K^*(1680)^0 \to K^+\pi^-$	<3.1	…
$K_2^*(1430)^0\pi^+$, $K_2^*(1430)^0 \to K^+\pi^-$	<2.3	…
$\rho(770)^0K^+$, $\rho(770)^0 \to \pi^+\pi^-$	$4.78 \pm 0.75 \pm 0.44^{+0.91}_{-0.87}$	$4.78 \pm 0.75 \pm 0.44^{+0.91}_{-0.87}$
$f_0(980)K^+$, $f_0(980) \to \pi^+\pi^-$	$7.55 \pm 1.24 \pm 0.69^{+1.48}_{-0.96}$	…
$f_2(1270)K^+$, $f_2(1270) \to \pi^+\pi^-$	<1.3	…
Nonresonant	…	$17.3 \pm 1.7 \pm 1.6^{+17.1}_{-7.8}$
$K^+K^+K^-$ charmless total	…	$30.6 \pm 1.2 \pm 2.3$
ϕK^+, $\phi \to K^+K^-$	$4.72 \pm 0.45 \pm 0.35^{+0.39}_{-0.22}$	$9.60 \pm 0.92 \pm 0.71^{+0.78}_{-0.46}$
$\phi(1680)K^+$, $\phi(1680) \to K^+K^-$	<0.8	
$f_0(980)K^+$, $f_0(980) \to K^+K^-$	<2.9	
$f_2'(1525)K^+$, $f_2'(1525) \to K^+K^-$	<4.9	
$a_2(1320)K^+$, $a_2(1320) \to K^+K^-$	<1.1	
Nonresonant	…	$24.0 \pm 1.5 \pm 1.8^{+1.9}_{-5.7}$
$\chi_{c0}K^+$, $\chi_{c0} \to \pi^+\pi^-$	$1.37 \pm 0.28 \pm 0.12^{+0.34}_{-0.35}$	…
$\chi_{c0}K^+$, $\chi_{c0} \to K^+K^-$	$0.86 \pm 0.26 \pm 0.06^{+0.20}_{-0.05}$	…
$\chi_{c0}K^+$ combined	…	$196 \pm 35 \pm 33^{+197}_{-26}$

TABLE VII. Contributions to the systematic uncertainty (in percent) for the three-body $B^+ \to K^+\pi^+\pi^-$ and $B^+ \to K^+K^+K^-$ branching fractions.

Source	Error	
	$K^+\pi^+\pi^-$	$K^+K^+K^-$
Efficiency nonuniformity	1.2	0.7
Event shape requirements	2.5	1.7
Signal yield extraction	5.4	2.1
PID	6.0	6.0
Charged track reconstruction	3.0	3.0
MC statistics	1.0	1.0
$N_{B\bar{B}}$ Estimation	1.0	1.0
Total	9.2	7.4

mated using pure samples of kaons and pions from $D^0 \to K^-\pi^+$ decays, where the D^0 flavor is tagged using $D^{*+} \to D^0\pi^+$. The systematic uncertainty in charged track reconstruction is estimated using partially reconstructed $D^* \to D\pi$ events and from comparison of the ratio of $\eta \to \pi^+\pi^-\pi^0$ to $\eta \to \gamma\gamma$ events in data and MC. The overall systematic uncertainty for the three-body branching fraction is estimated to be ±9.2% and ±7.4% for the $K^+\pi^+\pi^-$ and $K^+K^+K^-$ final states, respectively.

VIII. DISCUSSION AND CONCLUSION

With a 140 fb^{-1} data sample collected with the Belle detector, we have performed the first amplitude analysis of B meson decays to three-body charmless $K^+\pi^+\pi^-$ and $K^+K^+K^-$ final states. Clear signals are observed in the $B^+ \to K^*(892)^0\pi^+$, $B^+ \to \rho(770)^0K^+$, $B^+ \to f_0(980)K^+$ and $B^+ \to \phi K^+$ decay channels [26]. The model uncertainty for these channels is relatively small due to the narrow width of the intermediate resonances and (in vector-pseudoscalar decays) due to vector meson polarization which provides clear signal signatures.

The branching fraction measured for the decay $B^+ \to K^*(892)^0\pi^+$ is significantly lower than that reported earlier [6,9]. The simplified technique used for the analysis of the $B^+ \to K^+\pi^+\pi^-$ decay described in [6,9] has no sensitivity to the relative phases between different resonances, resulting in a large model error. The full amplitude analysis presented in this paper consistently treats effects of interference between quasi-two-body amplitudes thus reducing the model error. The analysis suggests the presence of an additional (presumably nonresonant) amplitude in the mass region of the $K^*(892)^0$ that absorbs a significant fraction of the B signal. The $B^+ \to K^*(892)^0\pi^+$ branching fraction measured in our analysis is in better agreement with theoretical predictions based on the QCD factorization approach [27].

The decay mode $B^+ \to f_0(980)K^+$ is the first observed example of a B decay to a charmless scalar-pseudoscalar final state. The mass $M(f_0(980)) = 976 \pm 4^{+2}_{-3}\ \mathrm{MeV}/c^2$ and width $\Gamma(f_0(980)) = 61 \pm 9^{+14}_{-8}\ \mathrm{MeV}/c^2$ obtained from the fit are in agreement with previous measurements [15]. To check the sensitivity of the results to the parametrization of the $f_0(980)$ lineshape, we repeat the fit with the Flatté lineshape [21]. In this case, because of limited statistics, we fix g_K at the value reported by the E791 Collaboration [28]: $g_K = 0.02 \pm 0.04 \pm 0.03$. Since the central value for g_K measured in [28] is consistent with zero, we also make a fit to data with g_K fixed at zero. Finally we repeat the fit with both g_π and g_K floated. In all cases we obtain consistent results. The sensitivity to the $B^+ \to f_0(980)K^+$ decay in the $K^+K^+K^-$ final state is greatly reduced by the large $B^+ \to \phi K^+$ amplitude and by the scalar nonresonant amplitude. No statistically significant contribution from this channel to the $K^+K^+K^-$ three-body final state is observed, thus only a 90% confidence level upper limit for the corresponding branching fractions product is reported.

We report the first observation of the decay $B^+ \to \rho(770)^0K^+$. The statistical significance [29] of the signal exceeds 6σ with all the models used to fit the $B^+ \to K^+\pi^+\pi^-$ signal. The measured branching fraction for this channel agrees well with the theoretical prediction in QCD factorization [27]. This is one of the channels where large direct *CP* violation is expected [27].

Because of the very narrow width of the ϕ meson, the branching fraction for the decay $B^+ \to \phi K^+$ is determined with a small model uncertainty. The obtained value is in good agreement with previous measurements [30].

A clear signal is also observed for the decay $B^+ \to \chi_{c0}K^+$ in both $\chi_{c0} \to \pi^+\pi^-$ and $\chi_{c0} \to K^+K^-$ channels. Although quite significant statistically, the $B^+ \to \chi_{c0}K^+$ signal constitutes only a small fraction of the total three-body signal and thus suffers from a large model error, especially in the $K^+K^+K^-$ final state, where the charmless nonresonant amplitude in the χ_{c0} mass region is enhanced compared to the $K^+\pi^+\pi^-$ final state due to the interference caused by the presence of the two identical kaons.

We also check possible contributions from $B^+ \to K_2^*(1430)^0\pi^+$, $B^+ \to K^*(1410)^0\pi^+$, $B^+ \to K^*(1680)^0\pi^+$, and $B^+ \to f_2(1270)K^+$ decays. In the $K^+K^+K^-$ final states we check for the $B^+ \to f_2'(1525)K^+$, $B^+ \to a_2(1320)K^+$, and $B^+ \to \phi(1680)K^+$ signals. We find no statistically significant signal in any of these channels. As a result, we set 90% confidence level upper limits for their branching fractions. In the factorization approximation, charmless B decays to pseudoscalar-tensor final states are expected to occur at the level of 10^{-6} or less [31].

For other quasi-two-body channels the interpretation of fit results is less certain. Although a signal for $B^+ \to K_0^*(1430)^0\pi^+$ is observed with a high statistical significance, its branching fraction is determined with a large model error. Two solutions with significantly different fractions of the $B^+ \to K_0^*(1430)^0\pi^+$ channel but similar likelihood values are obtained from the fit to $K^+\pi^+\pi^-$ events. Study with MC simulation confirms the presence of the second solution. We prepare MC pseudoexperiments where the $B^+ \to K^+\pi^+\pi^-$ signal is generated with the matrix element of model $K\pi\pi - C_0$ with parameters corresponding to one of the solutions. In both cases the second solution is found in the fit to MC samples. It is also worth mentioning that the two solutions exist with all the parameterizations of the nonresonant amplitudes we tested. This may indicate that in order to choose a unique solution additional external information is required. In this sense, the useful piece of information seems to be the phenomenological estimation of the $B^+ \to K_0^*(1430)^0\pi^+$ branching fraction. The analysis of B meson decays to scalar-pseudoscalar final states described in Ref. [32] suggests that the branching fraction for the $B^+ \to K_0^*(1430)^0\pi^+$ decay can be as large as 40×10^{-6}. Unfortunately, the predicted value suffers from a large uncertainty that is mainly due to uncertainty in calculation of the $K_0^*(1430)$ decay constant $f_{K_0^*}$. Different methods used to estimate $f_{K_0^*}$ [32,33] give significantly different results. We may also try to resolve the ambiguity by employing independent information from other experiments. For example, analysis of the real and imaginary parts of the amplitude separately may provide additional useful information. Following the idea by BaBar Collaboration [26] (see also discussion below), we employ LASS results on the partial wave analysis of the elastic $K - \pi$ scattering [34]. We compare the total scalar K-π amplitude [which is a sum of the $B^+ \to K_0^*(1430)^0\pi^+$ amplitude and the $K - \pi$ component of the nonresonant amplitude Eq. (11)] with that measured by LASS. From this comparison, we find that results of the best fit (model $K\pi\pi - \mathrm{C}_0$, solution I) to the $K^+\pi^+\pi^-$ signal events are in good qualitative agreement with the LASS data.

We cannot identify unambiguously the broad structures observed in the $M(\pi^+\pi^-) \simeq 1.3\ \mathrm{GeV}/c^2$ mass region in the $B^+ \to K^+\pi^+\pi^-$ decay denoted in our analysis as $f_X(1300)$ and at $M(K^+K^-) \simeq 1.5\ \mathrm{GeV}/c^2$ in the $B^+ \to K^+K^+K^-$ decay denoted as $f_X(1500)$. If approximated by a single resonant state, $f_X(1300)$ is equally well described by a scalar or vector amplitude. Analysis with higher statistics might allow a more definite conclusion. The best description of the $f_X(1500)$ is achieved with a scalar amplitude with mass and width determined from the fit consistent with $f_0(1500)$ states [15].

Amplitude analysis often suffers from uncertainties related to the nonunique parametrization of the decay amplitude. In our case such an uncertainty originates mainly from the parametrization of the nonresonant amplitude. In this analysis, we use a rather simplified empirical parametrization with a single parameter. In the study of the $B^+ \to K^+\pi^+\pi^-$ decay by the BaBar Collaboration [26] a different approach is used. In their analysis, an attempt is made to parametrize $K_0^*(1430)^0\pi^+$ and the nonresonant component by a single amplitude suggested by the LASS Collaboration to describe the scalar amplitude in elastic $K\pi$ scattering [34]. Although this approach is experimentally motivated, the use of the LASS parametrization is limited to the elastic region of $M(K\pi) \lesssim 2.0\ \mathrm{GeV}/c^2$. Besides, an additional amplitude (a complex constant) is still required for a satisfactory description of the data [26].

It is worth noting that fractions of the nonresonant decay in both $B^+ \to K^+\pi^+\pi^-$ and $B^+ \to K^+K^+K^-$ decays are comparable in size and comprise a significant fraction of the total three-body signals. Moreover, in the parametrization used in this analysis the numerical values of the parameter [parameter α in Eqs. (11) and (12)] for the $B^+ \to K^+\pi^+\pi^-$ and $B^+ \to K^+K^+K^-$ are very close. This may indicate that the nonresonant amplitudes in both final states have a common nature, and simultaneous analysis of these two decay modes may impose additional constraints. An attempt for such an analysis has been made in [35]. However, the proposed model considers only the $\pi - \pi$ component [a_2^{nr} in Eq. (11)] of the nonresonant amplitude and does not account for the K-π component [a_1^{nr} in Eq. (11)], while in our analysis we find that the $K - \pi$ component dominates (see Table IV).

In some cases the uncertainty in the parametrization of the nonresonant amplitude significantly affects the extraction of relative fractions of other quasi-two-body channels. Further theoretical progress in this field might allow reduction of this uncertainty.

Results of the $B^+ \to K^+K^+K^-$ Dalitz analysis can be also useful in connection with the measurement of CP violation in $B^0 \to K_S^0K^+K^-$ decay reported recently by the Belle [36] and BaBar [37] Collaborations. An isospin analysis of B decays to three-kaon final states by Belle [3] and independent analysis with moments technique [38] by BaBar [39] suggest the dominance of the CP-even component in the $B^0 \to K_S^0K^+K^-$ decay (after the $B^0 \to \phi K_S^0$ signal is excluded). This conclusion can be checked independently by an amplitude analysis of the $K_S^0K^+K^-$ final state, where the fraction of CP-odd states can be obtained as a fraction of states with odd orbital momenta. Unfortunately, such an analysis is not feasible with the current experimental data set. Nevertheless, the fact that we do not observe any significant vector amplitude other than $B^+ \to \phi K^+$ in the decay $B^+ \to K^+K^+K^-$ supports the conclusion.

ACKNOWLEDGMENTS

We thank the KEKB group for the excellent operation of the accelerator, the KEK Cryogenics group for the efficient operation of the solenoid, and the KEK computer group and the National Institute of Informatics for valuable computing and Super-SINET network support. We acknowledge support from the Ministry of Education, Culture, Sports, Science, and Technology of Japan and the Japan Society for the Promotion of Science; the Australian Research Council and the Australian Department of Education, Science and Training; the National Science Foundation of China under contract No. 10175071; the Department of Science and Technology of India; the BK21 program of the Ministry of Education of Korea and the CHEP SRC program of the Korea Science and Engineering Foundation; the Polish State Committee for Scientific Research under Contract No. 2P03B 01324; the Ministry of Science and Technology of the Russian Federation; the Ministry of Education, Science and Sport of the Republic of Slovenia; the National Science Council and the Ministry of Education of Taiwan; and the U.S. Department of Energy.

---

[1] G. Eilam, M. Gronau, and R. R. Mendel, Phys. Rev. Lett. **74**, 4984 (1995); S. Fajfer, R. J. Oakes, and T. N. Pham, Phys. Lett. B **539**, 67 (2002).
[2] N. G. Deshpande, N. Sinha, and R. Sinha, Phys. Rev. Lett. **90**, 061802 (2003); However, this method might not work in practice, as explained in M. Gronau, Phys. Rev. Lett. **91**, 139101 (2003).
[3] A. Garmash *et al.* (Belle Collaboration), Phys. Rev. D **69**, 012001 (2004).
[4] T. Gershon and M. Hazumi, Phys. Lett. B **596**, 163 (2004).
[5] K. Abe *et al.* (Belle Collaboration), Report No. BELLE-CONF-0317, 2003.
[6] A. Garmash *et al.* (Belle Collaboration), Phys. Rev. D **65**, 092005 (2002).
[7] E. Eckhart *et al.* (CLEO Collaboration), Phys. Rev. Lett. **89**, 251801 (2002).
[8] B. Aubert *et al.* (BaBar Collaboration), hep-ex/0206004; B. Aubert *et al.* (BaBar Collaboration), Phys. Rev. Lett. **91**, 051801 (2003).
[9] B. Aubert *et al.* (BaBar Collaboration), hep-ex/0303022.
[10] S. Kurokawa, Nucl. Instr. and Meth. In Phys. Res. A **499**, 1 (2003).
[11] A. Abashian *et al.*, Nucl. Instr. and Meth. In Phys. Res. A **479**, 117 (2002).
[12] R. Brun *et al.*, GEANT 3.21, CERN Report No. DD/EE/84-1, 1984.
[13] H. Albrecht *et al.* (ARGUS Collaboration), Phys. Lett. B **229**, 304 (1989).

[14] Events are generated with the CLEO group's QQ program http://www.lns.cornell.edu/public/CLEO/soft/QQ.

[15] Particle Data Group, K. Hagiwara *et al.*, Phys. Rev. D **66**, 10001 (2002) and 2003 off-year partial update for the 2004 edition (http://pdg.lbl.gov).

[16] R. H. Dalitz, Philos. Mag. **44**, 1068 (1953).

[17] See "Review of Charm Dalitz-Plot Analyses" by D. Asner in [15] and references therein.

[18] J. Blatt and V. Weisskopf, *Theoretical Nuclear Physics* (John Wiley & Sons, New York, 1952).

[19] M. Wirbel, B. Stech, and M. Bauer, Z. Phys. C **29**, 637 (1985).

[20] H. Pilkuhn, *The Interactions of Hadrons* (North-Holland, Amsterdam, 1967).

[21] S. M. Flatté, Phys. Lett. B **63**, 224 (1976).

[22] M. G. Kendall and A. Stuart, *The Advanced Theory of Statistics*, 2nd ed. (Hafner Publishing, New York, 1968).

[23] In Dalitz analysis of D meson three-body decays it is common to visualize results of the fit as projections on mass squared variables. Because of the large mass of the B meson, we find that visualization is more convenient in terms of mass variables.

[24] E. M. Aitala *et al.* (E791 Collaboration), Phys. Rev. Lett. **89**, 121801 (2002).

[25] Note that $B^+ \to \chi_{c0} K^+$ channel is excluded while calculating branching fraction for the total $B^+ \to K^+ \pi^+ \pi^-$ and $B^+ \to K^+ K^+ K^-$ three-body charmless decays.

[26] At the time of the preparation of this manuscript for publication, preliminary results on amplitude analysis of $B^+ \to K^+ \pi^+ \pi^-$ decay have been reported by BaBar Collaboration: hep-ex/0408032. All the quasi-two-body branching fraction results from Belle and BaBar analyses are in good agreement. The comparison of relative phases is more uncertain due to differences in signal parametrizations and limited statistics.

[27] See for example: M. Beneke and M. Neubert, Nucl. Phys. **B675**, 333 (2003); C.-W. Chiang, M. Gronau, Z. Luo, J. L. Rosner, and D. A. Suprun, Phys. Rev. D **69**, 034001 (2004) and references therein.

[28] E. M. Aitala *et al.* (E791 Collaboration), Phys. Rev. Lett. **86**, 765 (2001).

[29] Statistical significance of the signal is calculated as $\sqrt{-2\ln(\mathcal{L}_0/\mathcal{L}_{\max})}$, where $\mathcal{L}_{\max}$ and $\mathcal{L}_0$ denote the maximum likelihood with the nominal signal yield and with the signal yield fixed at zero, respectively.

[30] B. Aubert *et al.* (BaBar Collaboration), Phys. Rev. Lett. **87**, 151801 (2001);K.-F. Chen, A. Bozek *et al.* (Belle Collaboration), Phys. Rev. Lett. **91**, 201801 (2003).

[31] C. S. Kim, B. H. Lim, and S. Oh, Eur. Phys. J. C **22**, 683 (2002); C. S. Kim, J. P. Lee, and S. Oh, Phys. Rev. D **67**, 014002 (2003).

[32] V. L. Chernyak, Phys. Lett. B **509**, 273 (2001).

[33] K. Maltman, Phys. Lett. B **462**, 14 (1999).

[34] D. Aston *et al.* Nucl. Phys. **B296**, 493 (1988).

[35] W. Ochs and P. Minkowski, Eur. Phys. J. C **39**, 71 (2005).

[36] K. Abe *et al.* (Belle Collaboration), Phys. Rev. Lett. **91**, 261602 (2003); K. Abe *et al.* (Belle Collaboration), hep-ex/0409049.

[37] B. Aubert *et al.* (BaBar Collaboration), Phys. Rev. Lett. **93**, 181805 (2004).

[38] M. Pivk and F. R. Le Diberder, physics/0402083.

[39] B. Aubert *et al.* (BaBar Collaboration), hep-ex/0408076.